Electromagnetic scattering by an aggregate of spheres: Theoretical and experimental study of the amplitude scattering matrix

Yu-lin Xu
Department of Astronomy, P.O. Box 112055, University of Florida, Gainesville, Florida 32611-2055

Ru T. Wang
Technology Applications Group, 3440 Quinn Ridge Drive, Snellville, Georgia 30039

(Received 25 February 1998; revised manuscript received 23 June 1998)

An accurate analytical representation of the amplitude scattering matrix is of key importance in the development of a reliable electromagnetic scattering formulation, because it enables one to derive rigorous analytical expressions for all scattering quantities. We compare a rigorous theory of scattering by aggregates of spheres [Y.-I. Xu, Appl. Opt. **36**, 9496 (1997)] with a large set of laboratory microwave analog scattering measurements for multiple spheres obtained by Wang between 1968 and 1983. Close agreement is found for all of the experimental data tested, confirming that the four amplitude scattering matrix elements can be accurately evaluated by the theory that is based on a far-field solution. It also leads to the validation of a simplified noninteracting-scattering (NIS) approximation derived from the theory. [S1063-651X(98)15209-1]

PACS number(s): 42.68.Mj, 92.60.Ta, 94.10.Gb

I. INTRODUCTION

Since the development of the scalar and vector addition theorems for spherical harmonics by Friedman and Russek [1], Stein [2], and Cruzan [3], many researchers, starting with Liang and Lo [4] and Bruning and Lo [5,6], have devoted considerable efforts to tackling the problem of light scattering by an arbitrary multisphere configuration analytically [7–19].

In a light-scattering theory, the most important and fundamental scattering quantity is the 2×2 amplitude scattering matrix, which completely defines the linear transformation between the incident and the scattered far-field amplitudes. Its analytical representation enables one to derive rigorous expressions for all scattering characteristics, such as the cross sections for extinction, scattering, absorption, and radiation pressure [20]. Moreover, the amplitude scattering matrix is closely related to the 4×4 scattering matrix, known as the Müller matrix, which describes precisely the linear relation between the incident and the scattered Stokes parameters. All of the 16 elements of the Müller matrix can be obtained directly from the amplitude scattering matrix [20]. A set of analytical expressions for the four elements of the amplitude scattering matrix of an arbitrary aggregate of spheres was first given by Xu [17], based on the so-called reexpansion method to obtain a single-field expansion of the total scattered field from the entire aggregate as a whole [17,18]. This reexpansion method encounters severe numerical problems in its practical applications [18]. Xu has recently developed a far-field approach to solving multisphere-scattering problems and has rederived the analytical expressions for the amplitude scattering matrix from the far-field solution [18]. We verify this theoretical development by comparing with the results of a set of laboratory microwave analog scattering measurements. Since 1968 onward to 1987, Wang [21–30] experimentally investigated the scattering properties of nonspherical, nonisotropic particles of various shapes, sizes, and dielectric properties, including a number of linear chains, dumbbells, and other aggregates of spheres using a 3-cm microwave scattering facility over several locations in Troy, New York (before 1970), Albany, New York (1970s), and Gainesville, Florida (after 1980). The extensive measurements accumulated three types of data for multiple spheres: (1) polarized scattered intensities as a function of scattering angle θ in a range from $0°$ to $170°$ for fixed and random orientations, (2) the variation of scattered intensities with particles' azimuthal angle, observed at a fixed scattering angle and a fixed polarization, and (3) the complex amplitude scattering matrix measured at the incident beam direction ($\theta=0°$). A few previous authors [11,12,17–19,31,32] have compared their theoretical calculations with some of these scattering measurements. We confirm our new formulation for the amplitude scattering matrix of an aggregate of particles by the systematic experimental validation using Wang's large set of laboratory data.

Section II gives a review of Xu's relevant theoretical work, especially those excerpted from the paper on the far-field solution [18], and presents the explicit forms of the amplitude scattering matrix elements. Expressions for pertinent scattering quantities, such as extinction efficiency and scattering intensity, all derivable from the matrix, are also given. Section III provides the simplification of the expressions given in Sec. II when each sphere in an aggregate is assumed to act independently of each other, i.e., for the noninteracting-scattering (NIS) case. Section IV briefs the microwave analog method and the techniques employed. Section V, which is divided into three subsections, illustrates in graphical forms the comparisons between theory and experiment. Theoretical results shown are from both the rigorous and the NIS solutions. Some explanations on the comparisons, coded target ID numbers, symbols and abbreviations are also included in Sec. V. Finally, Sec. VI gives conclusions.

II. AMPLITUDE SCATTERING MATRIX: ANALYTICAL REPRESENTATION

Cooperative scattering by an aggregate of spheres depends on the direction of the incident radiation, the sizes and

compositions of the component spheres, and the configuration and orientation of the aggregate. Consider an arbitrarily configured aggregate of L small homogeneous and isotropic spheres of an arbitrary combination of size and composition. In a primary reference system, in which (x,y,z) and (r,θ,ϕ) are as usual the Cartesian or the spherical polar coordinates, the aggregate is illuminated by a z-propagating plane wave with a linear polarization angle β, and the Cartesian coordinates of the center of each jth component sphere are denoted by (X^j,Y^j,Z^j). The partial (or called differential) scattering coefficients (a^j_{mn},b^j_{mn}), i.e., the expansion coefficients of the individual scattered fields from each component sphere associated with respective sphere-centered, displaced coordinate systems, can be solved in a linear system set up by the standard electromagnetic boundary conditions on the spherical surfaces of all component spheres through the generalization of the Mie theory [17]:

$$a^j_{mn}+a^j_n\sum_{l\neq j}^{(1,L)}\sum_{\nu=1}^{N^l}\sum_{\mu=-\nu}^{\nu}(A^{lj}_{mn\mu\nu}a^l_{\mu\nu}+B^{lj}_{mn\mu\nu}b^l_{\mu\nu})=a^j_np^j_{mn}, \tag{1a}$$

$$b^j_{mn}+b^j_n\sum_{l\neq j}^{(1,L)}\sum_{\nu=1}^{N^l}\sum_{\mu=-\nu}^{\nu}(B^{lj}_{mn\mu\nu}a^l_{\mu\nu}+A^{lj}_{mn\mu\nu}b^l_{\mu\nu})=b^j_nq^j_{mn}, \tag{1b}$$

where $j=1,2,\cdots,L$, $|m|\leqslant n$, $n=1,2,\ldots,N^j$. Literally, $N^l=\infty$. But in practical calculations, the field expansions must be truncated at some sufficiently high scattering orders. The well-known criterion [20,33] for the field-expansion truncation of a single sphere with size parameter x^j, $N^j\approx x^j+4\sqrt[3]{x^j}+2$, is generally satisfactory for all the component spheres in the solution of Eqs. (1). a^j_n and b^j_n in Eqs. (1) are the Mie scattering coefficients of the isolated jth component sphere [20,34,35]. p^j_{mn} and q^j_{mn}, the expansion coefficients of the incident field expressed in the jth coordinate system centered on the jth sphere, are given by [17,18]

$$p^j_{mn}=\exp(ikZ^j)p^0_{mn},\quad q^j_{mn}=\exp(ikZ^j)q^0_{mn}, \tag{2}$$

where $i=\sqrt{-1}$, k is the wave number, $p^0_{mn}=q^0_{mn}=0$ except $|m|=1$, and [17,18]

$$p^0_{1n}=q^0_{1n}=\frac{\exp(-i\beta)}{2},\quad p^0_{-1n}=-q^0_{-1n}=-\frac{\exp(i\beta)}{2n(n+1)}. \tag{3}$$

$A^{lj}_{mn\mu\nu}$ and $B^{lj}_{mn\mu\nu}$ in Eqs. (1) are the vector translation coefficients associated with the translation vector extended from the origin of the lth coordinate system to the origin of the jth coordinate system. These translation coefficients are based on the Hankel function of the first kind, characterizing the transformation of outgoing elementary spherical waves in the lth coordinate system into incoming waves in the jth coordinate system. The detailed discussion about the analytical representation of these vector addition coefficients and about the necessary numerical techniques in their evaluation can be found elsewhere [2,3,36–40]. As mentioned earlier, in describing scattering characteristics of scatterers, the fundamental scattering quantity is the 2×2 complex amplitude scattering matrix. It describes the linear relation between the incident and the scattered far-field components that are parallel and perpendicular to the scattering plane defined by the direction of propagation of the plane incident wave and the scattering direction,

$$\begin{pmatrix}E_{\parallel s}\\E_{\perp s}\end{pmatrix}=\frac{\exp[ik(r-z)]}{-ikr}\begin{pmatrix}S_2&S_3\\S_4&S_1\end{pmatrix}\begin{pmatrix}E_{\parallel i}\\E_{\perp i}\end{pmatrix}. \tag{4}$$

For the case of a plane z-propagating incident wave under our consideration,

$$E_{\parallel i}=E_0(\cos\phi\cos\beta+\sin\phi\sin\beta), \tag{5a}$$

$$E_{\perp i}=E_0(\sin\phi\cos\beta-\cos\phi\sin\beta), \tag{5b}$$

Eq. (4) becomes

$$\begin{pmatrix}E_{s\theta}\\-E_{s\phi}\end{pmatrix}=\frac{E_0\exp[ik(r-z)]}{-ikr}\begin{pmatrix}S_2&S_3\\S_4&S_1\end{pmatrix}\begin{bmatrix}\cos(\phi-\beta)\\\sin(\phi-\beta)\end{bmatrix}. \tag{6}$$

In general, the amplitude scattering matrix is a function of both the scattering angle θ and the azimuthal angle ϕ. Based on the far-field solution to the multisphere-scattering problem, Xu [18] recently showed that the four elements of the amplitude scattering matrix of an aggregate of spheres in Eq. (6) can be rigorously expressed by the following equations in terms of the partial scattering coefficients (a^l_{mn},b^l_{mn}) and the geometry of the aggregate:

$$S_2(\theta,\phi)=\sum_{l=1}^{L}\exp(-ik\Delta^l)\sum_{n=1}^{N^l}\sum_{m=0}^{n}\frac{2n+1}{1+\delta_{0m}}\{\Psi^l_{mn}\cos[(m-1)\phi+\beta]+i\Phi^l_{mn}\sin[(m-1)\phi+\beta]\}, \tag{7a}$$

$$S_3(\theta,\phi)=\sum_{l=1}^{L}\exp(-ik\Delta^l)\sum_{n=1}^{N^l}\sum_{m=0}^{n}\frac{2n+1}{1+\delta_{0m}}\{i\Phi^l_{mn}\cos[(m-1)\phi+\beta]-\Psi^l_{mn}\sin[(m-1)\phi+\beta]\}, \tag{7b}$$

$$S_4(\theta,\phi)=\sum_{l=1}^{L}\exp(-ik\Delta^l)\sum_{n=1}^{N^l}\sum_{m=0}^{n}\frac{2n+1}{1+\delta_{0m}}\{-i\Theta^l_{mn}\cos[(m-1)\phi+\beta]+\Xi^l_{mn}\sin[(m-1)\phi+\beta]\}, \tag{7c}$$

$$S_1(\theta,\phi)=\sum_{l=1}^{L}\exp(-ik\Delta^l)\sum_{n=1}^{N^l}\sum_{m=0}^{n}\frac{2n+1}{1+\delta_{0m}}\{\Xi_{mn}^l\cos[(m-1)\phi+\beta]+i\Theta_{mn}^l\sin[(m-1)\phi+\beta]\},\tag{7d}$$

where δ_{0m} is the Krönecker delta symbol, $\Delta^l=X^l\sin\theta\cos\phi+Y^l\sin\theta\sin\phi+Z^l\cos\theta$,

$$\Psi_{mn}^l=\frac{(n-m)!}{(n+m)!}(a_{mn}^l\tau_{mn}+b_{mn}^l\pi_{mn})+(-1)^m(a_{-mn}^l\tau_{mn}-b_{-mn}^l\pi_{mn}),\tag{8a}$$

$$\Phi_{mn}^l=\frac{(n-m)!}{(n+m)!}(a_{mn}^l\tau_{mn}+b_{mn}^l\pi_{mn})-(-1)^m(a_{-mn}^l\tau_{mn}-b_{-mn}^l\pi_{mn}),\tag{8b}$$

$$\Theta_{mn}^l=\frac{(n-m)!}{(n+m)!}(a_{mn}^l\pi_{mn}+b_{mn}^l\tau_{mn})-(-1)^m(a_{-mn}^l\pi_{mn}-b_{-mn}^l\tau_{mn}),\tag{8c}$$

$$\Xi_{mn}^l=\frac{(n-m)!}{(n+m)!}(a_{mn}^l\pi_{mn}+b_{mn}^l\tau_{mn})+(-1)^m(a_{-mn}^l\pi_{mn}-b_{-mn}^l\tau_{mn}),\tag{8d}$$

the angular functions are defined by

$$\pi_{mn}(\cos\theta)=\frac{m}{\sin\theta}P_n^m(\cos\theta),\qquad \tau_{mn}(\cos\theta)=\frac{d}{d\theta}P_n^m(\cos\theta),\tag{9}$$

and P_n^m is the associated Legendre function of the first kind of degree n and order m.

With the amplitude scattering matrix rigorously known, the explicit formulas for the extinction and scattering cross sections and the asymmetry parameter of an ensemble of particles can be derived through the equations [20,41]

$$C_{\rm ext}=\frac{4\pi}{k^2}\mathrm{Re}[(\mathbf{V}\cdot\hat{\mathbf{e}}_{\mathbf{v}})_{\theta=0}],\quad C_{\rm sca}=\int_0^{2\pi}\int_0^{\pi}\frac{|\mathbf{V}|^2}{k^2}\sin\theta d\theta d\phi,\tag{10a}$$

$$\langle\cos\theta\rangle=\int_0^{2\pi}\int_0^{\pi}\frac{|\mathbf{V}|^2}{k^2C_{\rm sca}}\cos\theta\sin\theta d\theta d\phi,\tag{10b}$$

where $\mathbf{V}$ is the vector scattering amplitude related to the scalar scattering amplitude by

$$\mathbf{V}=[S_2\cos(\phi-\beta)+S_3\sin(\phi-\beta)]\hat{\mathbf{e}}_{\boldsymbol{\theta}}-[S_4\cos(\phi-\beta)+S_1\sin(\phi-\beta)]\hat{\mathbf{e}}_{\boldsymbol{\phi}},\tag{11}$$

and $\hat{\mathbf{e}}_{\mathbf{v}}=\sin\theta\cos(\phi-\beta)\hat{\mathbf{e}}_r+\cos\theta\cos(\phi-\beta)\hat{\mathbf{e}}_{\boldsymbol{\theta}}-\sin(\phi-\beta)\hat{\mathbf{e}}_{\boldsymbol{\phi}}$ with $(\hat{\mathbf{e}}_r,\hat{\mathbf{e}}_\theta,\hat{\mathbf{e}}_\phi)$ being the basis unit vectors associated with the spherical polar coordinate system (r,θ,ϕ). The rigorous analytical expressions for the extinction and scattering cross sections and the asymmetry parameter derived from Eqs. (10) with (7) and (11) have been given in Refs.[18] and [19].

Of interest to practical problems are often the scattering calculations or measurements in a single scattering plane. Without loss of generality, the x-z plane ($\phi=0°$) is usually defined as the scattering plane. Also, of particular interest to many practical applications are often the two typical polarization states of the plane incident wave: $\beta=0°$ and $\beta=90°$, i.e., the plane incident wave is x or y polarized. When $\phi=0°$, Eqs. (7) reduce to the form for $\beta=0°$,

$$S_2^x(\theta)=\sum_{l=1}^{L}\exp(-ik\Delta^l)\sum_{n=1}^{N^l}\sum_{m=0}^{n}\frac{2n+1}{1+\delta_{0m}}\Psi_{mn}^l,\tag{12a}$$

$$S_3^x(\theta)=i\sum_{l=1}^{L}\exp(-ik\Delta^l)\sum_{n=1}^{N^l}\sum_{m=0}^{n}\frac{2n+1}{1+\delta_{0m}}\Phi_{mn}^l,\tag{12b}$$

$$S_4^x(\theta)=-i\sum_{l=1}^{L}\exp(-ik\Delta^l)\sum_{n=1}^{N^l}\sum_{m=0}^{n}\frac{2n+1}{1+\delta_{0m}}\Theta_{mn}^l,\tag{12c}$$

$$S_1^x(\theta)=\sum_{l=1}^{L}\exp(-ik\Delta^l)\sum_{n=1}^{N^l}\sum_{m=0}^{n}\frac{2n+1}{1+\delta_{0m}}\Xi_{mn}^l,\tag{12d}$$

and for $\beta=90°$,

$$S_2^y(\theta)=i\sum_{l=1}^{L}\exp(-ik\Delta^l)\sum_{n=1}^{N^l}\sum_{m=0}^{n}\frac{2n+1}{1+\delta_{0m}}\Phi_{mn}^l,\tag{13a}$$

$$S_3^y(\theta)=-\sum_{l=1}^{L}\exp(-ik\Delta^l)\sum_{n=1}^{N^l}\sum_{m=0}^{n}\frac{2n+1}{1+\delta_{0m}}\Psi_{mn}^l,\tag{13b}$$

$$S_4^y(\theta)=\sum_{l=1}^{L}\exp(-ik\Delta^l)\sum_{n=1}^{N^l}\sum_{m=0}^{n}\frac{2n+1}{1+\delta_{0m}}\Xi_{mn}^l,\tag{13c}$$

$$S_1^y(\theta)=i\sum_{l=1}^{L}\exp(-ik\Delta^l)\sum_{n=1}^{N^l}\sum_{m=0}^{n}\frac{2n+1}{1+\delta_{0m}}\Theta_{mn}^l,\tag{13d}$$

where superscript x or y indicates the polarization state of the plane incident wave.

Forward scattering properties are described fully by the complex scattering amplitude $S(0°)$ at the forward direction of $\theta=0°$. At this particular scattering direction,

$$\pi_{mn}=\tau_{mn}=0,\quad |m|\neq 1,\tag{14a}$$

$$\pi_{1n}=\tau_{1n}=n(n+1)/2, \tag{14b}$$

and from Eqs. (8) we have

$$\Psi^l_{mn}(0^\circ)=\Xi^l_{mn}(0^\circ)=\Phi^l_{mn}(0^\circ)=\Theta^l_{mn}(0^\circ)=0, \quad m\neq 1, \tag{15a}$$

$$\Psi^l_{1n}(0^\circ)=\Xi^l_{1n}(0^\circ) =[a^l_{1n}+b^l_{1n}-n(n+1)(a^l_{-1n}-b^l_{-1n})]/2, \tag{15b}$$

$$\Phi^l_{1n}(0^\circ)=\Theta^l_{1n}(0^\circ) =[a^l_{1n}+b^l_{1n}+n(n+1)(a^l_{-1n}-b^l_{-1n})]/2. \tag{15c}$$

From Eqs. (7), (14), and (15) it is obvious that the ϕ dependence of the scattering matrix elements automatically goes away at $\theta=0^\circ$ because only the modes of $m=1$ remain in this particular case. The dimensionless complex scattering amplitude $S(0^\circ)$ of an aggregate of spheres is thus given by

$$S(0^\circ)=(\mathbf{V}\cdot\hat{\mathbf{e}}_v)_{\theta=0}=S_2(0^\circ)=S_1(0^\circ) =\frac{1}{2}\sum_{l=1}^{L}\exp(-ikZ^l)\sum_{n=1}^{N^l}(2n+1)[(a^l_{1n}+b^l_{1n}) \times\exp(i\beta)-n(n+1)(a^l_{-1n}-b^l_{-1n})\exp(-i\beta)], \tag{16}$$

which is independent of the angle ϕ. For the two particular cases of $\beta=0^\circ$ or 90°, i.e., in which the plane incident wave is x or y polarized, Eq. (16) becomes

$$S^x(0^\circ)=\frac{1}{2}\sum_{l=1}^{L}\exp(-ikZ^l)\sum_{n=1}^{N^l}(2n+1) \times[a^l_{1n}+b^l_{1n}-n(n+1)(a^l_{-1n}-b^l_{-1n})], \tag{17a}$$

$$S^y(0^\circ)=\frac{i}{2}\sum_{l=1}^{L}\exp(-ikZ^l)\sum_{n=1}^{N^l}(2n+1)[a^l_{1n}+b^l_{1n} +n(n+1)(a^l_{-1n}-b^l_{-1n})]. \tag{17b}$$

It is convenient to present both theoretical and experimental results of the complex forward scattering amplitude $S(0^\circ)$ in the form of a Cartesian representation of (P,Q). In the complex plane, the dimensionless P and Q components of $S(0^\circ)$ are, respectively,

$$P=\frac{4\pi}{k^2G}\mathrm{Im}[S(0^\circ)], \quad Q=\frac{4\pi}{k^2G}\mathrm{Re}[S(0^\circ)], \tag{18}$$

where G is the sum of the geometric cross sections of the component spheres, which is the geometric cross section of a surface-equivalent single sphere, and Q is the (surface-equivalent) extinction efficiency. GQ is the extinction cross section C_{ext} of the entire aggregate.

III. LIGHT SCATTERING BY NONINTERACTING SPHERES

If a component sphere in an aggregate has no (or negligible) interaction with all other spheres in the aggregate, i.e., the sphere acts as a Mie-scatterer independent of others, the differential scattering coefficients of the sphere [see Eqs. (1)] become [17,18]

$$a^l_{mn}=p^l_{mn}a^l_n, \quad b^l_{mn}=q^l_{mn}b^l_n, \tag{19}$$

because in this case all the terms involving vector translation coefficients $A^{lj}_{mn\mu\nu}$ and $B^{lj}_{mn\mu\nu}$ in Eqs. (1) vanish or they are negligible. Inserting Eqs. (2) and (3) into Eqs. (19), we have

$$a^l_{mn}=b^l_{mn}=0, \quad |m|\neq 1, \tag{20a}$$

$$a^l_{1n}=\frac{a^l_n}{2}\exp[i(kZ^l-\beta)], \quad b^l_{1n}=\frac{b^l_n}{2}\exp[i(kZ^l-\beta)], \tag{20b}$$

$$a^l_{-1n}=-\frac{a^l_n}{2n(n+1)}\exp[i(kZ^l+\beta)],$$

$$b^l_{-1n}=\frac{b^l_n}{2n(n+1)}\exp[i(kZ^l+\beta)], \tag{20c}$$

which, by way of Eqs. (8), lead to

$$\Psi^l_{1n}=\frac{\exp(ikZ^l)}{n(n+1)}(a^l_n\tau_n+b^l_n\pi_n)\cos\beta, \tag{21a}$$

$$\Phi^l_{1n}=\frac{\exp(ikZ^l)}{n(n+1)}(a^l_n\tau_n+b^l_n\pi_n)(-i\sin\beta), \tag{21b}$$

$$\Theta^l_{1n}=\frac{\exp(ikZ^l)}{n(n+1)}(a^l_n\pi_n+b^l_n\tau_n)(-i\sin\beta), \tag{21c}$$

$$\Xi^l_{1n}=\frac{\exp(ikZ^l)}{n(n+1)}(a^l_n\pi_n+b^l_n\tau_n)\cos\beta, \tag{21d}$$

where $\pi_n=\pi_{1n}$, $\tau_n=\tau_{1n}$. If the interactions among component spheres in an aggregate are all negligible, it can be shown from Eqs. (7), (8), (16), (20), and (21) that, for this noninteracting scattering,

$$S_2(\theta)=\sum_{l=1}^{L}\exp[ik(Z^l-\Delta^l)]\sum_{n=1}^{N^l}\frac{2n+1}{n(n+1)}(a^l_n\tau_n+b^l_n\pi_n) =\sum_{l=1}^{L}\exp[ik(Z^l-\Delta^l)]\hat{S}^l_2(\theta), \tag{22a}$$

$$S_3(\theta)=S_4(\theta)=0, \tag{22b}$$

$$S_1(\theta)=\sum_{l=1}^{L}\exp[ik(Z^l-\Delta^l)]\sum_{n=1}^{N^l}\frac{2n+1}{n(n+1)}(a^l_n\pi_n+b^l_n\tau_n) =\sum_{l=1}^{L}\exp[ik(Z^l-\Delta^l)]\hat{S}^l_1(\theta), \tag{22c}$$

$$S(0°)=S^x(0°)=S^y(0°)$$
$$=\frac{1}{2}\sum_{l=1}^{L}\sum_{n=1}^{N^l}(2n+1)(a_n^l+b_n^l)=\sum_{l=1}^{L}\hat{S}^l(0°), \tag{22d}$$

where $\hat{S}_2^l(\theta)$, $\hat{S}_1^l(\theta)$, and $\hat{S}^l(0°)$ refer to Mie scattering from the isolated lth sphere. In this case of scattering by an ensemble of noninteracting spheres, the complex forward-scattering amplitude of the ensemble depends solely on the sizes and the compositions of the component spheres and is irrelevant to the configuration and orientation of the ensemble. Especially, the values of P and Q of an ensemble of noninteracting identical spheres are exactly the same as those of the single component sphere. This coherent Mie scattering applies to an aggregate with sufficiently large separations between all component spheres. It is also a good approximation to an aggregate for which the number and the maximum size of the component spheres are both sufficiently small and interaction between spheres is sufficiently weak. Equation (22d) shows that the complex forward-scattering amplitude (and therefore the total extinction cross section) of an ensemble of noninteracting spheres is just the simple sum of those of all the component spheres. However, even with the interaction turned off, the phase function, i.e., the angular distribution of the scattered intensity of an ensemble of spheres still strongly depends on the geometric pattern of the ensemble, totally different from those of the individual component spheres, as shown explicitly in Eqs. (22a) and (22c).

For illustration, we consider the simplest sphere system—two identical spheres. The center-to-center separation distance between the two spheres is d. Just for convenience in the following discussion, we locate one of the two sphere centers at the origin of the primary coordinate system. The axis of symmetry of the bisphere system lies in the scattering plane defined by the x-z plane and makes an angle χ with the z axis, i.e., with the direction of propagation of the plane incident wave. From Eqs. (22a) and (22c) it follows that the dependence of scattering by such two noninteracting spheres on the scattering angle θ and the orientation χ can be expressed in a simple form. Here, $\phi=0°$, $Z^{(1)}=\Delta^{(1)}=0$, $X^{(2)}=d\sin\chi$, $Z^{(2)}=d\cos\chi$, $\Delta^{(2)}=d(\sin\chi\sin\theta+\cos\chi\cos\theta)$, and

$$S_2(\theta)=(1+\exp\{ikd[\cos\chi-\cos(\chi-\theta)]\})\hat{S}_2(\theta), \tag{23a}$$

$$S_3(\theta)=S_4(\theta)=0, \tag{23b}$$

$$S_1(\theta)=(1+\exp\{ikd[\cos\chi-\cos(\chi-\theta)]\})\hat{S}_1(\theta), \tag{23c}$$

where $\hat{S}_2(\theta)$ and $\hat{S}_1(\theta)$ are the amplitude-scattering-matrix elements of the individual Mie sphere. Similar notations are employed for the intensity components: $\hat{i}_{11}(\theta)=|\hat{S}_1(\theta)|^2$ and $\hat{i}_{22}(\theta)=|\hat{S}_2(\theta)|^2$. For both the perpendicular- and parallel-to-the-scattering-plane polarized components, the *ratio* of the intensity from the two-sphere array to that from an individual component sphere is therefore given by the same function:

$$f(\theta,\chi)=\frac{i_{11}(\theta)}{2\hat{i}_{11}(\theta)}=\frac{i_{22}(\theta)}{2\hat{i}_{22}(\theta)}$$
$$=1+\cos\left[2kd\,\sin\left(\frac{\theta}{2}\right)\sin\left(\chi-\frac{\theta}{2}\right)\right]. \tag{24}$$

Thus in the particular case of NIS by two identical spheres, *this ratio is independent of the size and the composition of the component sphere, is symmetric about* $\chi=\theta/2$, *and has its maximum at* $\chi=\theta/2$. Notice also that this function $f(\theta,\chi)$ corresponds to the *form factor* in a special Rayleigh-Gans scattering [20,34,35], where it is as if the scattering volume degenerated into two geometrical points at the respective two sphere centers, from which two coherent waves possessing the component sphere's Mie fields were emitted and were combined vectorially to the resulting scattering pattern.

IV. METHOD OF SCATTERING MEASUREMENT

The microwave analog scattering measurement method [28–30] derives its merits from an important statement deduced from the principle of electrodynamic similitude [42]: *the physics of a scattering process depends only upon the ratio of particle size to wavelength*. This allows us to investigate, e.g., visible light scattering from micron or submicron particles by studying instead a microwave-wavelength (we use $\lambda=3.1835$cm) scattering from proportionately scaled-up, cm-sized particles. One is then capable of precisely knowing or controlling virtually all the scattering parameters, such as particle size, shape, refractive index, orientation in the beam, etc. Our microwave analog scattering measurement technique has advantages in many aspects. First, the true scattering signal from a particle, even in the beam direction ($\theta=0°$), can be extracted out of that mixed with the coherent background (null technique). Second, near $\theta=0°$ both the amplitude and phase of scattered wave can be measured simultaneously, which, in turn, make it possible to directly determine total cross sections. Examples are given in Figs. 28–33 in the form of (P,Q) plots. Third, the magnitude of an observed scattering can be calibrated using a standard target of known magnitude by running it in a quick succession to the particle being measured, i.e., *normalization is not needed* in our data.

The scattering targets are manufactured by either molding or machining commercially available plastic materials. Molding also allows us to control the target's refractive index $m(=m'+im'')$, by varying the density of target medium and/or admixing it with other materials such as carbon dusts. The refractive index of a target is determined from the complex dielectric constant $\varepsilon(=\varepsilon'+i\varepsilon'')$ measurement of rectangular waveguide samples prepared from the same target medium, using the classical standing-wave method [29,43]. m and ε are related by the Maxwell's relation $m^2=\varepsilon$.

The scattering facility employs a tight incident beam from a parabolic transmitter antenna, and two similar narrow beam receiving antennas. This is to minimize measurement errors caused by stray reflections from the laboratory ceiling, floor, and side walls even though critical portions of each are lined with microwave absorbing materials. A fixed receiver antenna in the beam direction ($\theta=0°$) is for extinction measurement, and a movable antenna around the target site is for

angular scattering in a range of scattering angle $5° \leqslant \theta \leqslant 170°$ [28–30]. In both measurements the microwave-unique ''null technique'' is employed to discriminate the desired target-scattered wave against the unwanted background wave: In the absence of target in the beam, the unwanted background wave is combined with a nulling wave that is piped through a separate waveguide. Both the amplitude and phase of this nulling wave are then adjusted to cancel the background wave. The off-balance from this established null status when the target is brought into position is therefore the desired target-scattered wave.

To precisely position and orient a particle in the beam had been one of the most difficult tasks in our microwave measurements. We refer the details to in the earlier publications, and mention here that only nylon strings are used for either the manually operated mechanism or the computer-driven device.

In order to obtain orientation-averaged extinction and/or angular scattering data, we let a particle step through all preselected orientations while keeping it in the beam center, and record the data at each of these orientations. The average is simply the arithmetic mean of these data. We assume that the nulling made at the outset of the run suffers little drift during this orientation-stepping period (typically ~ 2 min for a $\theta = 0°$ run, and ~ 5 min for other θ's). This assumption is not always valid, however, especially for the measurements near $\theta = 0°$. This is because near $\theta = 0°$ beam direction we have a very large unwanted background (the direct wave from the transmitter), the intensity of which is ~ 1000 times that of a typical 2″-diam-sphere's $\theta = 0°$ scattering. A slight ambient change (e.g., temperature variation) could produce a significant null drift the magnitude of which is comparable to or even larger than the target-scattered signal itself. To minimize such drift-caused errors we employed highly frequency-stabilized microwave source, carefully designed null-waveguide path length, performed extinction measurement at early morning hours when environment conditions are most stable, and discarded those data whose stability records were not acceptable. Yet, unnoticed such errors could show up during a run, especially for small particles. At other scattering angles, on the other hand, null drifts present much less problems. This is because by unpublished background-radiation surveys on each of our scattering chambers, we noted that the unwanted background intensity levels were at least 50 dB lower than the $\theta = 0°$ maxima when $\theta \geqslant 20°$, while angular scattering intensities of our particles had in general less than 30 dB variations from their respective $\theta = 0°$ peaks.

V. COMPARISON BETWEEN THEORY AND EXPERIMENT

A. Angular distribution

In 1983, Wang and Gustafson [27] reported the microwave analog scattering measurement results for phase functions and the degree of polarization of the scattered radiation from various linear chains of spheres, each consisting of two, three, or five identical components, the physical and geometrical parameters of which are listed in Table I. A six-digit ID number was assigned to each linear chain for identification (see Table I). The first digit is exclusively 5, the second indicates the size of the component sphere (a larger number for a larger size), the third denotes the number of spheres in the chain, and the remaining three digits start with two zeros followed by a number indicating the intersphere separation, e.g., ''0'' means that the neighboring spheres are in contact. The scattering measurements include three polarization components of the scattered intensity at each scattering angle: i_{11}, i_{22}, and i_{12}. Here the first suffix refers to the incident polarization and the second to that of the received radiation, with ''1'' and ''2'' denoting perpendicular and parallel to the (horizontal) scattering plane, respectively. At each of the three polarization settings, the target (the aggregate of spheres) was controlled to step through 44 orientations in the beam while the scattered intensity was recorded at each step, of which 35 are uniformly distributed over an octant of space and the rest are some preferred special orientations. The arithmetic mean of the recorded intensities over the 35 orientations is taken as the averaged intensity over random orientations.

TABLE I. Target parameters of the sphere aggregates in Wang's phase function measurements.

Target ID No.	No. of spheres	Size parameter of single sphere	Refractive index	Separation parameter
	n	x	$m' - im''$	kd[a]
532 000	2	3.083	$1.61 - i0.004$	6.166
532 001	2	3.083	$1.61 - i0.004$	8.030
532 004	2	3.083	$1.61 - i0.004$	12.51
533 001	3	3.083	$1.61 - i0.004$	7.52
535 001	5	3.083	$1.61 - i0.004$	7.76
542 000	2	4.346	$1.63 - i0.010$	8.693
542 001	2	4.346	$1.63 - i0.010$	9.94
542 001	2	4.346	$1.63 - i0.010$	10.76

[a] d is the center-to-center separation distance between each pair of neighboring spheres and k is the free-space wave number of the incident radiation.

We compare our calculation results with the measurement for both the principal fixed orientations and the random-orientation average. Our theoretical calculations for i_{11}, i_{22}, and i_{12} use the equations

$$i_{11}(\theta) = |S_1^y(\theta)|^2, \quad i_{22}(\theta) = |S_2^x(\theta)|^2, \quad i_{12}(\theta) = |S_3^y(\theta)|^2, \tag{25}$$

where $S_1^y(\theta)$, $S_2^x(\theta)$, and $S_3^y(\theta)$ are given by Eqs. (13d), (12a), and (13b), respectively. Cooperative scattering by an ensemble of particles includes the interaction effect arising from the multiple scattering among individual particles and the far-field interference between scattered waves from individual particles. In addition to the exact multisphere-scattering calculations, which take into account both effects rigorously, we also calculated the NIS, i.e., the coherent Mie scattering for the case of an aggregate of spheres, which considers the interference effect only. In the coherent Mie-scattering calculations for i_{11} and i_{22} using Eqs. (25), $S_1(\theta)$ and $S_2(\theta)$ are given by Eqs. (22a) and (22c), respectively, independent of the polarization state of the plane incident wave.

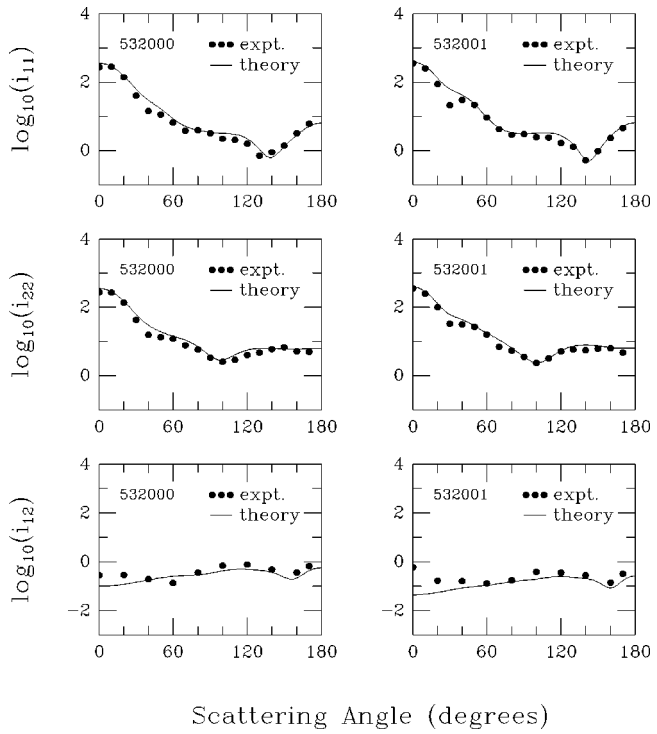

FIG. 1. Comparison of theoretical predictions from Xu's rigorous solution of multisphere light-scattering problems (theory) with Wang's laboratory microwave analog scattering measurements (expt.) for angular distribution of the polarization components of scattered intensity, i_{11}, i_{22}, and i_{12} by two randomly oriented linear chains of spheres, ID Nos. 532 000 and 532 001 (see Table I). The three panels in the left column refer to 532 000 and the three in the right column for 532 001.

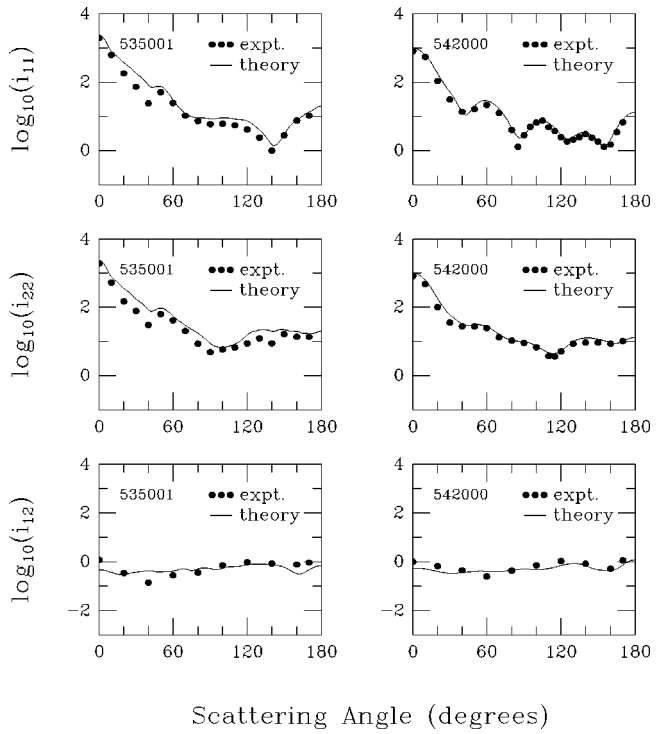

FIG. 3. Same as Fig. 1, but for target ID No. 535 001 (left column) and 542 000 (right column).

1. Random orientations

Figures 1–4 compare our theoretical predictions from the rigorous multisphere-scattering theory with laboratory measurement results of i_{11}, i_{22}, and i_{12} on a random-orientation average for the eight sphere chains listed in Table I, which show a good agreement between theory and experiment. To

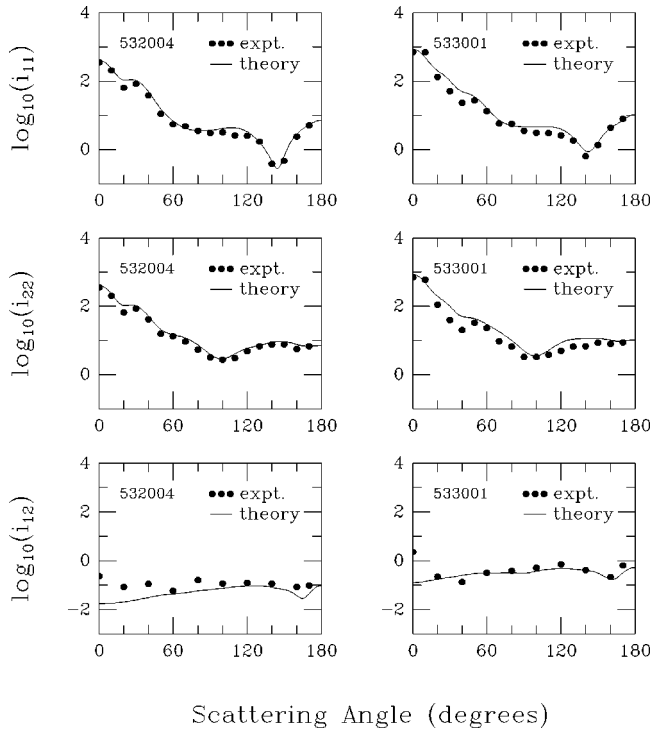

FIG. 2. Same as Fig. 1, but for target ID Nos. 532 004 (left column) and 533 001 (right column).

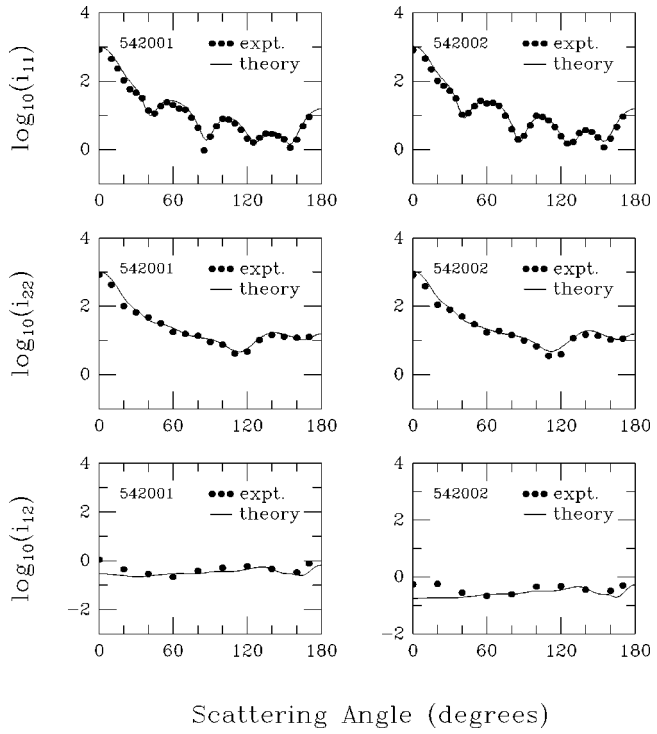

FIG. 4. Same as Fig. 1, but for target ID Nos. 542 001 (left column) and 542 002 (right column).

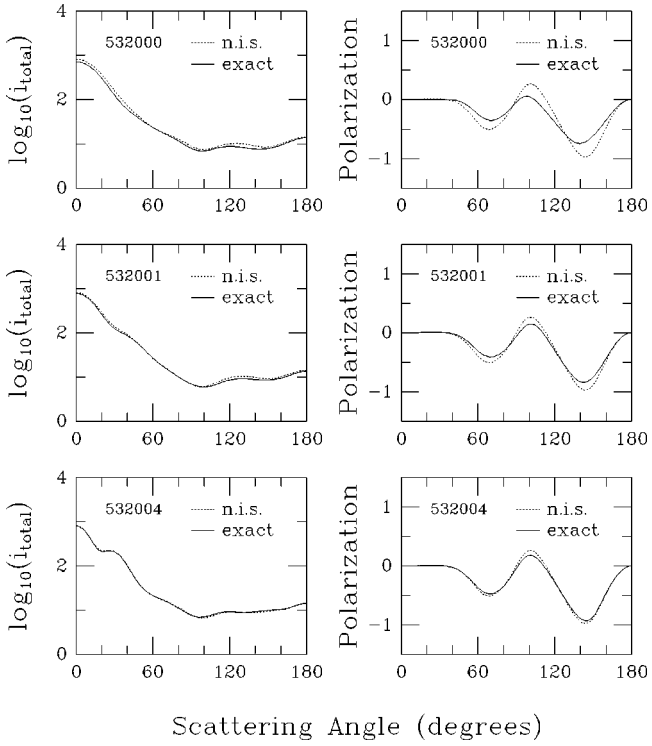

FIG. 5. Comparison of Xu's rigorous solution (exact) with NIS approximations (n.i.s.) for angular distribution of the total scattered intensity, $i_{\text{total}}=(i_{11}+i_{22})/2$, and the polarization, $p=(i_{11}-i_{22})/(i_{11}+i_{22})$, by three randomly oriented linear chains of spheres, ID Nos. 532 000, 532 001, and 532 004 (see Table I).

examine the contribution from interaction between spheres, we also compare rigorous solution with coherent Mie scattering for all the eight chains of spheres in Figs. 5–7, wherein we employ the notations: $i_{\text{total}}=(i_{11}+i_{22})/2$, and the polarization $p=(i_{11}-i_{22})/(i_{11}+i_{22})$. These figures do not include i_{12} since it does not exist for coherent Mie-scattering. The difference between rigorous solution (solid curves) and coherent Mie-scattering (dotted curves) is attributed to the interaction effect. From Figs. 5 and 7 we clearly see that interaction weakens with the increase in intersphere separation and with the decrease in component sphere size. The

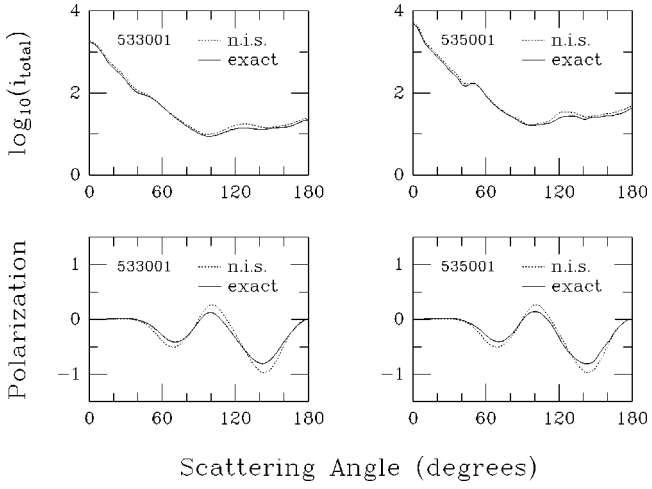

FIG. 6. Similar to Fig. 5, but for target ID Nos. 533 001 (left column) and 535 001 (right column).

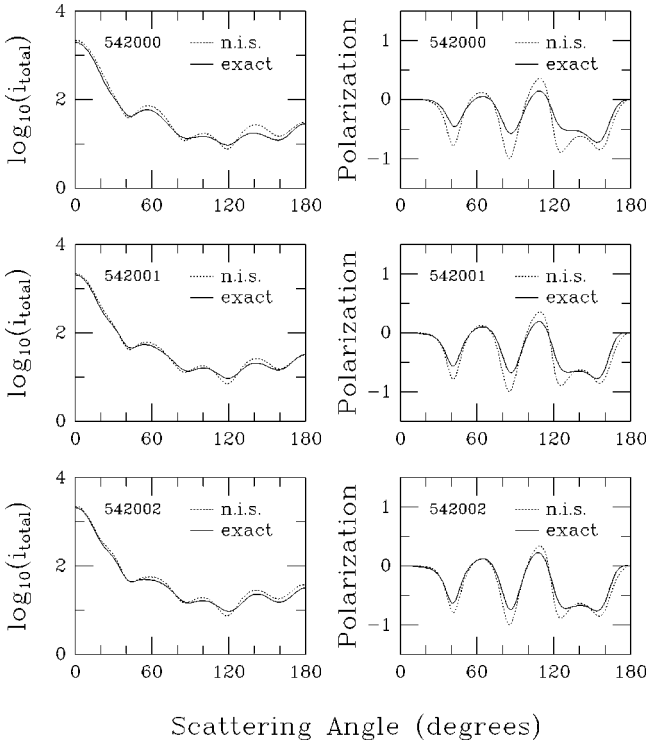

FIG. 7. Same as Fig. 5, but for target ID Nos. 542 000, 542 001, and 542 002.

three bisphere systems in each of the two groups, (532 000, 532 001, 532 004) or (542 000, 542 001, 542 002), consist of the same two identical spheres but with different intersphere separations. Each individual sphere in the former group has a size parameter of 3.083 and a complex refractive index of $1.61-i0.004$ while for the latter group the size parameter is 4.346 and the refractive index is $1.63-i0.01$. The two spheres in 532 000 or 542 000 are in contact and have stronger interaction than others in the same group. Also, the two spheres in 542 000 show stronger interaction than those in 532 000 because of their larger size parameter. But for all the eight chains of spheres, the interaction between spheres is generally weak when random-orientation average is considered, especially the dumbbels 532 004 and 542 002 whose component spheres are rather separated.

It is noted that, in Figs. 1–4, the measured i_{12} near $\theta=0°$ is always higher than theoretical prediction. The reason for this has been mentioned in the last paragraph of Sec. IV. As seen from the figures, i_{12} is generally a few magnitudes smaller than i_{11} and i_{22}. In laboratory microwave measurement, the measured signal includes both true signal and residual noise background even though the unwanted background wave can be mostly canceled through the use of the null technique. The residual background intensity level could be comparable to or much higher than the scattered intensity signal i_{12} itself. For this reason, the accuracy of measurement for i_{12} is usually poorer than that for i_{11} and i_{22}, especially at the scattering angles near $\theta=0°$, where the residual background noise level is at least 50 dB higher than at other scattering angles.

Figures 1–4 show that the theoretical predictions for the scattered intensities generally agree with laboratory data in terms of the detailed running-trend-matching of the curves.

TABLE II. Average and maximum relative deviations, $\overline{\delta}$(%) and δ_{max}(%), of the orientation-averaged i_{11} and i_{22} of the eight chains of spheres (listed in Table I) in Wang's laboratory microwave scattering measurements from theoretical predictions.

Target ID No.	$\overline{\delta}(i_{11})$	$\overline{\delta}(i_{22})$	$\delta_{max}(i_{11})$	$\delta_{max}(i_{22})$
532 000	−12.80	−18.13	−51.02	−47.38
532 001	−15.54	−15.01	−65.53	−45.17
532 004	−15.96	−16.14	−40.41	−36.99
533 001	−17.35	−28.50	−51.69	−59.48
535 001	−29.80	−36.09	−69.83	−62.67
542 000	−14.63	−14.83	−47.72	−43.58
542 001	−13.09	−8.33	−54.01	−42.28
542 001	−6.72	−12.28	−38.61	−37.04

TABLE III. Relative deviations, δ(%), of the orientation-averaged i_{11} and i_{22} of the eight chains of spheres (listed in Table I) at $\theta=0°$ and $\theta=170°$ in Wang's laboratory microwave scattering measurements from theoretical predictions.

Target ID No.	$\delta(i_{11}(0°))$	$\delta[i_{22}(0°)]$	$\delta[i_{11}(170°)]$	$\delta[i_{22}(170°)]$
532 000	−21.78	−21.78	21.76	−18.77
532 001	−7.27	−7.27	−9.28	−25.51
532 004	−10.73	−10.73	−4.82	−0.04
533 001	−15.51	−15.51	10.29	−7.02
535 001	−16.67	−16.67	−19.38	−18.56
542 000	−15.61	−15.61	−15.97	3.18
542 001	−17.78	−17.78	−11.25	11.12
542 001	−22.44	−22.44	−9.09	−0.58

Profiles of the intensity curves are sensitive to size, refractive index, and the configuration of the spheres. This kind of graphical comparison, mainly used in the present paper, is a reliable approach to mutually testing theoretical and experimental results. Nevertheless, comparison of theory with experiment can also be put on a quantitative basis. We calculated the relative deviations of i_{11} and i_{22} for all the eight chains of spheres. The relative deviation is defined by

$$\frac{(\text{laboratory measurement})-(\text{rigorous solution})}{(\text{rigorous solution})}.$$

The relative deviations, especially those of 532 000, 533 001 and 535 001, are mostly negative. This is because the gain factors used in the calibration of these experimental data sets are slightly too small. As mentioned in Sec. IV, the intensity measurements in each run for a range of scattering angles from 0° to 170° are calibrated using a ''standard sphere'' of known magnitude by measuring its scattered intensity at a carefully selected scattering angle right after the run. The ''gain factor,'' which is the calculated-to-measured intensity ratio of the standard sphere at the specific scattering angle, is used as the single constant calibration factor for the entire set of measurement. All the recorded intensities at different scattering angles in the same set are multiplied by the same calibration factor to obtain final ''absolute'' measurement results. This process of calibration does not change the profile of the measured intensity curve at all but scales up or down all the recorded intensities. Statistically, if the number of measurement points is sufficiently large and the calibration factor is sufficiently accurate, the average relative deviation should be sufficiently close to zero. The average deviations of the measured i_{11} and i_{22} of the eight chains of spheres, together with their respective maximum deviations in each of the data sets, are listed in Table II. The relative deviations at two particular scattering angles $\theta=0°$ and $\theta=170°$ are shown in Table III. After we adjust the calibration factor for a set of measurement data so that the average relative deviation goes to zero, the relative deviations will change slightly by exactly the same small amount. The same is for the experimental data points shown in Figs. 1–4 but the resulting shift will be nearly unnoticeable in the logarithmic scale, at less than or around 0.1. Compared with the corresponding original measurements, the experimental curves of i_{11} and i_{22} after adjustment will have exactly the same profiles, while uplifted slightly. Our calculations show that the typical level of the relative deviations of the measured i_{11} and i_{22} of the eight chains of spheres is about 10–20% for the majority of the measurements, whereas it is above 50% for a few individual points.

In the comparison between theory and experiment, both graphical and quantitative methods can be used. For our pur-

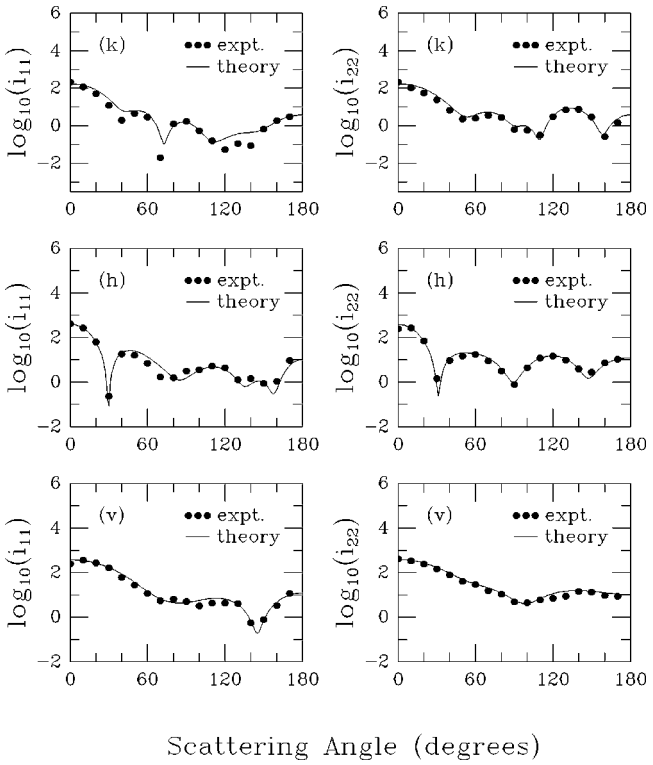

FIG. 8. Comparison of theoretical predictions from Xu's rigorous solution (theory) with Wang's microwave analog scattering measurements (expt.) for angular distribution of the polarization components of scattered intensity, i_{11} and i_{22}, of the linear chain of spheres, ID No. 532 000 (see Table I), in three principal fixed orientations, k, h, and v. k means that the axis of symmetry of the spheres is parallel to the plane incident beam direction. For h, the axis of symmetry lies in the scattering plane and is perpendicular to the incident beam direction, and for v, it is perpendicular to both the scattering plane and the incident beam direction.

pose of testing theory, the graphical comparison between theoretical and experimental results is probably more convenient and intuitive.

2. Single orientations

For each of the eight chains of spheres listed in Table I, Figs. 8–15 display the comparisons of the calculated and measured i_{11} and i_{22} at three principal fixed orientations. These three principal orientations (k,h,v) are defined by the orientation of the sphere-chain's axis of symmetry in the reference system, when it is aligned along the z, x, and y axes, respectively. In the same way as defined elsewhere in the present paper, the z axis coincides with the plane incident beam direction and the x-z plane is the scattering plane. For all three single orientations of (k,h,v) and for all eight chains of spheres, the agreement between theoretical calculations and experimental results is, again, generally good in terms of scattering-pattern matching in the graphical form. For the relative deviations of the measured i_{11} and i_{22} from theoretical predictions, compared to the case of random orientations discussed in the previous subsection, there are individual measurements showing larger deviations from theoretical calculation in this case of fixed orientations. This is largely due to (1) the deviation of the actual orientation of the target from the specified orientation and (2) the low scattered intensities at some scattering angles located at or near a local minimum. It is obvious that precise positioning of the target orientation is more important in a fixed-orientation measurement than orientation averaging. Also, the scattered intensity curves of a fixed orientation may have fine structures, ripples, and local minima and maxima, which would be smeared out in an average over orientations. For certain scattering angles, the scattered intensities at a fixed orientation may be quite small near the region of a local minimum, especially for backscattering, for which small absolute errors in measurement result in large fractional errors.

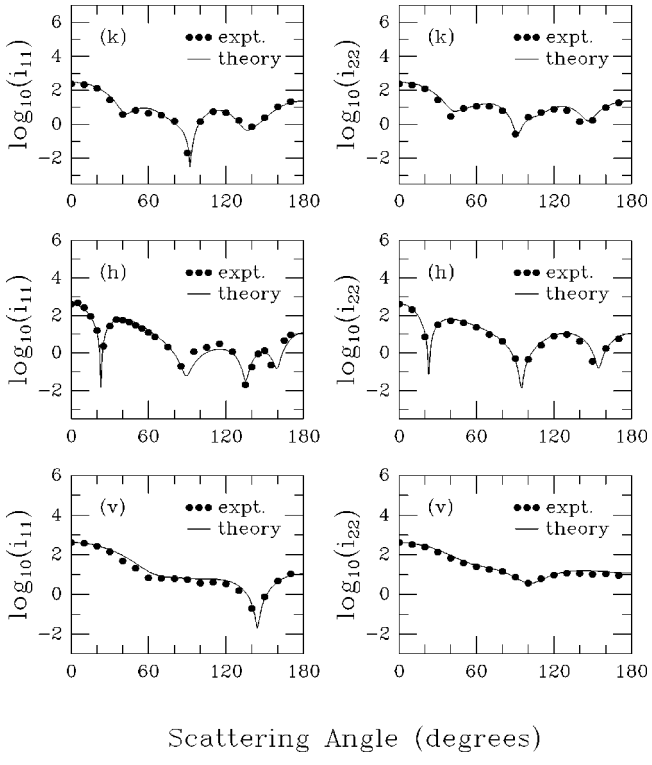

FIG. 9. Same as Fig. 8, but for the target ID No. 532 001 (see Table I).

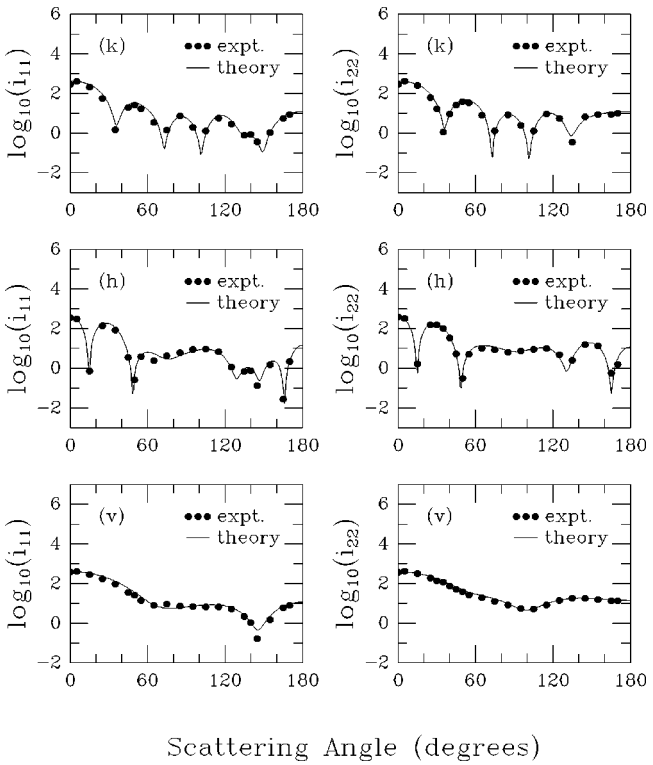

FIG. 10. Same as Fig. 8, but for the target ID No. 532 004 (see Table I).

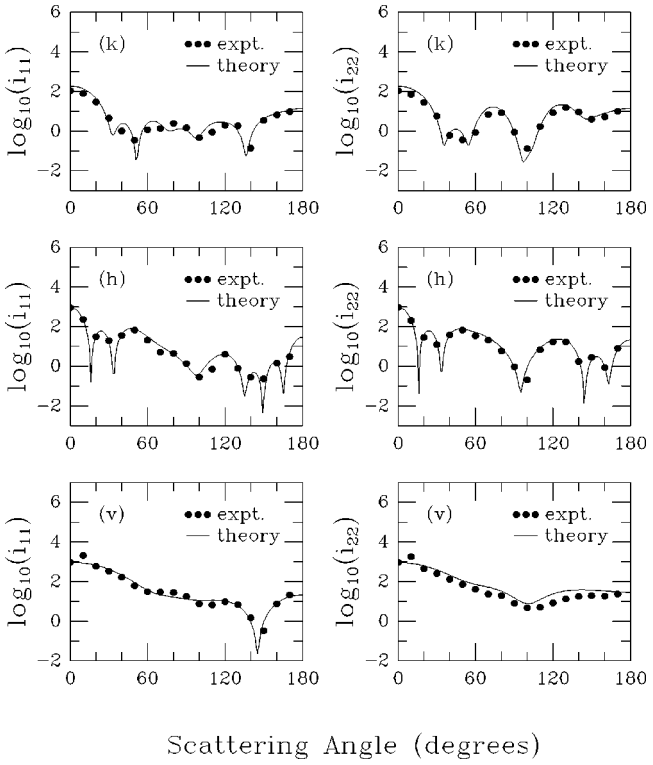

FIG. 11. Same as Fig. 8, but for the target ID No. 533 001 (see Table I).

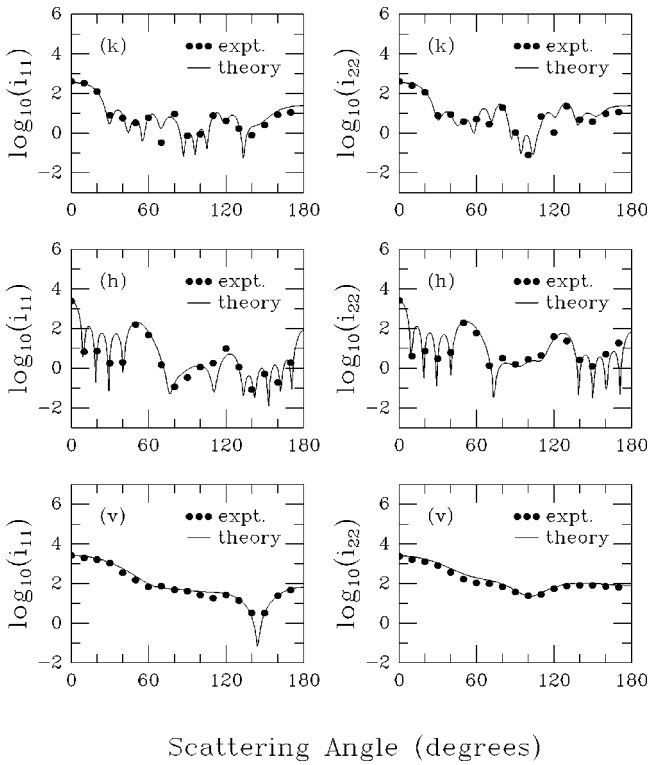

FIG. 12. Same as Fig. 8, but for the target ID No. 535 001 (see Table I).

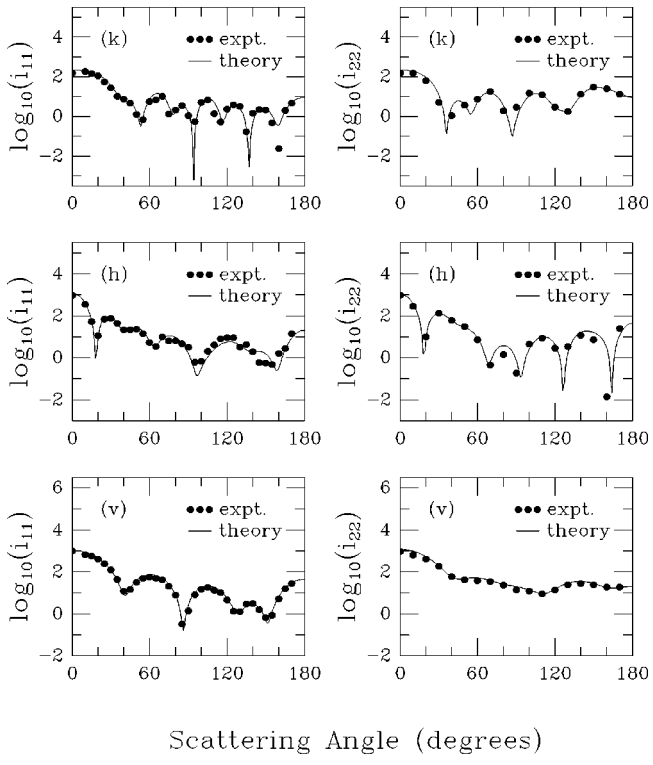

FIG. 14. Same as Fig. 8, but for the target ID No. 542 001 (see Table I).

Similar to the discussions for random orientations, Figs. 16–23 compare rigorous solution with coherent Mie scattering NIS that excludes the interaction effect for the three fixed orientations. These comparisons reveal that the interaction between spheres is strong in the orientation of k and that it is weak in the orientation of v. These comparisons show that (1) the rigorous solution and the noninteracting approximation are significantly different when the spheres are aligned

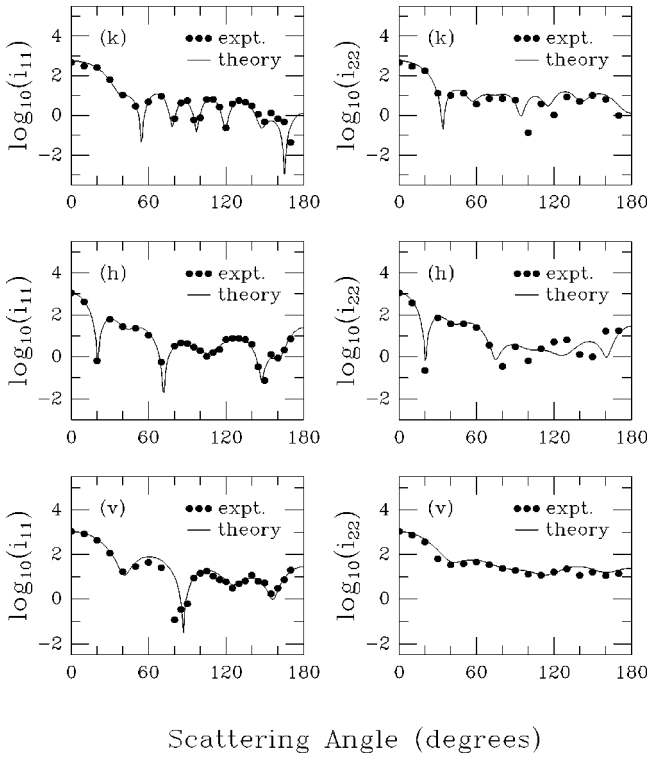

FIG. 13. Same as Fig. 8, but for the target ID No. 542 000 (see Table I).

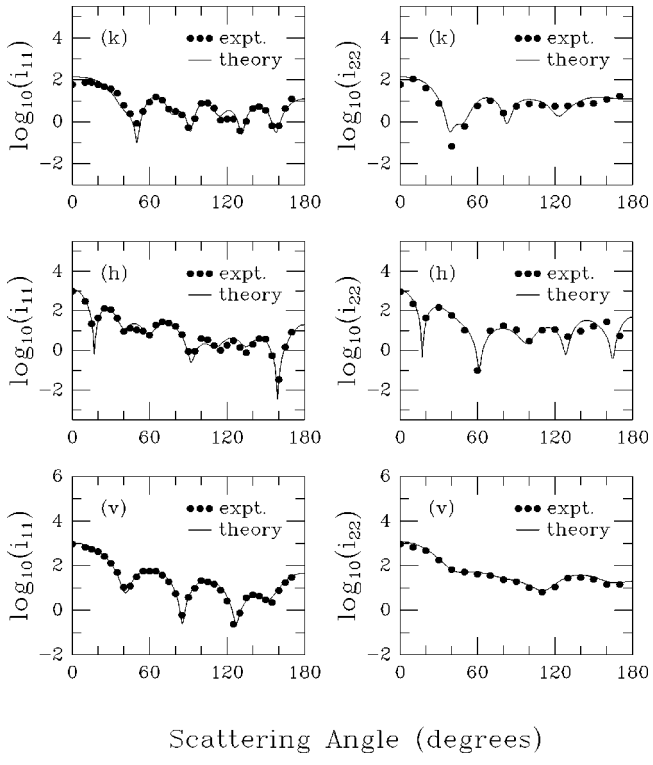

FIG. 15. Same as Fig. 8, but for the target ID No. 542 002 (see Table I).

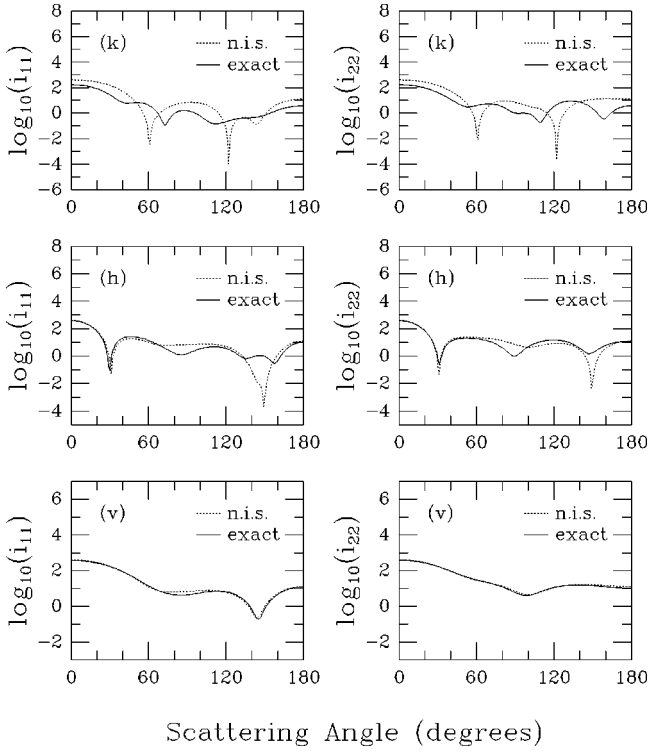

FIG. 16. Comparison of Xu's rigorous solution (exact) with NIS approximation (n.i.s.) for angular distribution of i_{11} and i_{22} of the linear chain of spheres, ID No. 532 000 (see Table I), in three principal fixed orientations, k, h, and v. k means that the axis of symmetry of the spheres is parallel to the plane incident beam direction. For h, the axis of symmetry lies in the scattering plane and is perpendicular to the incident beam direction, and for v, it is perpendicular to both the scattering plane and the incident beam direction.

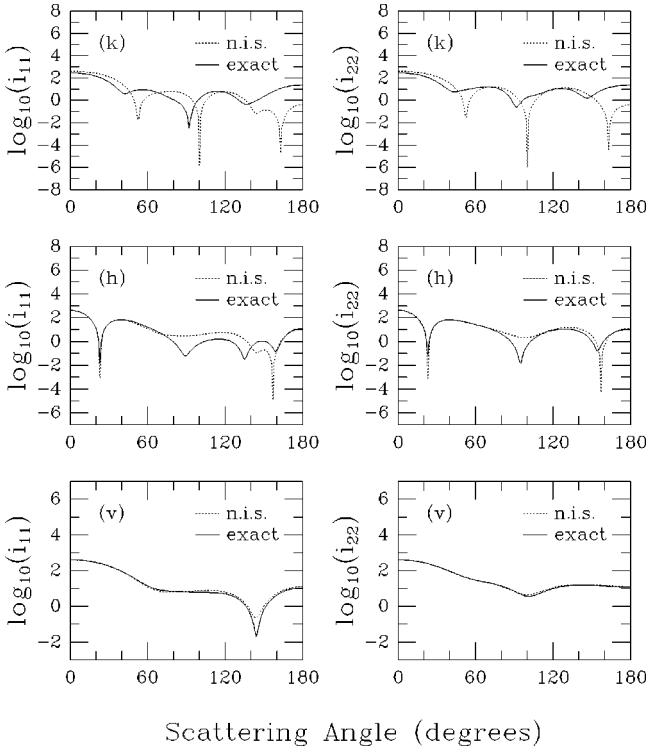

FIG. 17. Same as Fig. 16, but for the target ID No. 532 001 (see Table I).

along the incident beam direction, i.e., in the case of k, (2) the rigorous solution can be well duplicated by the noninteracting approximation for all scattering angles in the case of v, and (3) the two solutions are similar only for the forward scattering at $\theta\sim 0°$ and for the backscattering at $\theta\sim 180°$ in the case of h. These can be interpreted in terms of Eqs. (7), the analytical expressions for the amplitude scattering matrix elements. Scattering by many particles consists of two effects: interaction and far-field interference between scattered waves from individual particles. If there is no or very weak interaction between spheres, the rigorous and the noninteracting-scattering solutions should be identical or nearly identical. Due to interaction between spheres the interactive scattering coefficients (a_{mn}^l, b_{mn}^l) of each lth sphere differ from those determined by its Mie-scattering coefficients by way of Eqs. (19). These interactive scattering coefficients appear in Eqs. (7) in a combination with the phase factor $\exp(-ik\Delta^l)$, where $\Delta^l = X^l \sin\theta\cos\phi + Y^l \sin\theta \sin\phi + Z^l \cos\theta$. For the case of a single scattering plane we discussed here, $\phi = 0°$, therefore, $\Delta^l = X^l \sin\theta + Z^l \cos\theta$, which does not involve Y^l. For the orientation of v, $Z^l \equiv X^l \equiv 0$, which leads to $\Delta^l \equiv 0$, indicating that there is no interference between the scattered waves from component spheres. In this orientation, the scattering pattern of the entire aggregate of identical spheres is the same as that from an individual sphere when the interaction between spheres is negligible, every component sphere retaining the same scattered Mie field because $Z^l \equiv 0$. The Mie solutions (with the number of spheres taken into account) are identical to the coherent Mie-scattering in this case. For the orientation of h, $Z^l \equiv 0$, $\Delta^l = X^l \sin\theta$. When $\theta\sim 0°$ or $\theta\sim 180°$, $\Delta^l \sim 0$, which implies

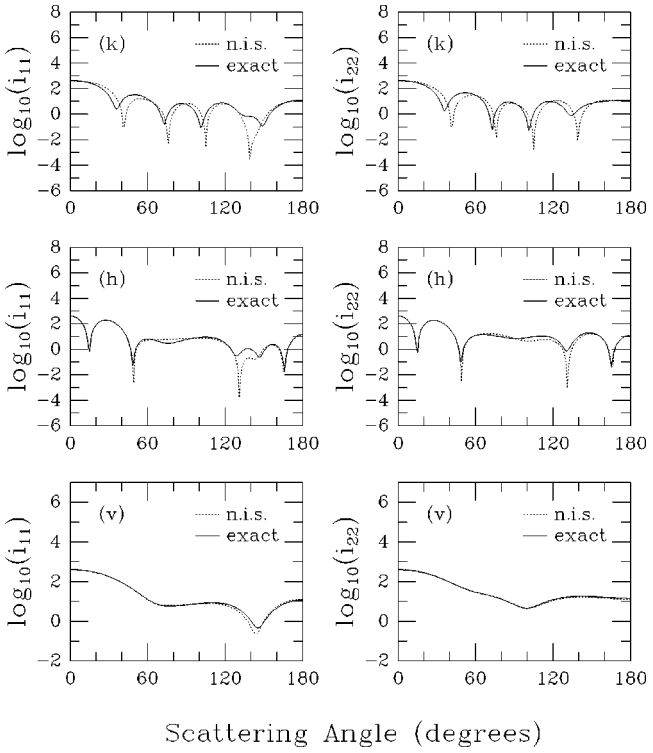

FIG. 18. Same as Fig. 16, but for the target ID No. 532 004 (see Table I).

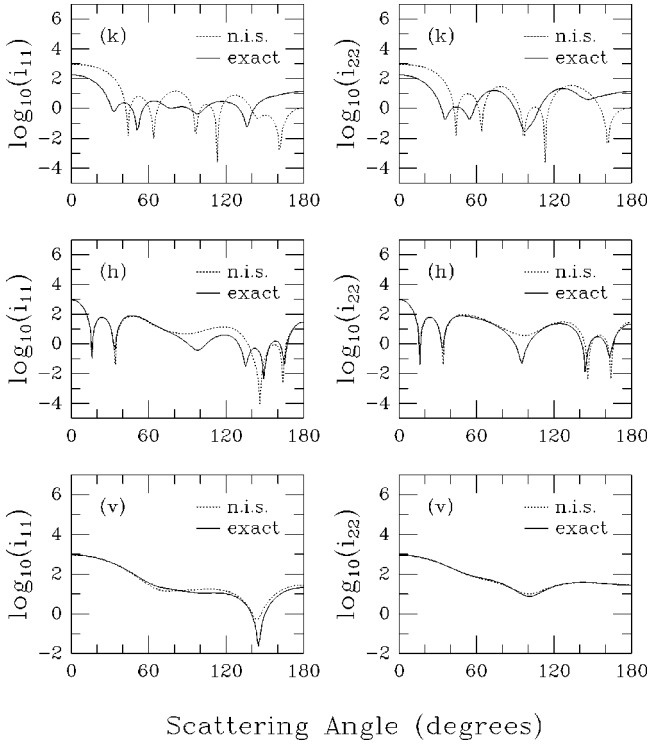

FIG. 19. Same as Fig. 16, but for the target ID No. 533 001 (see Table I).

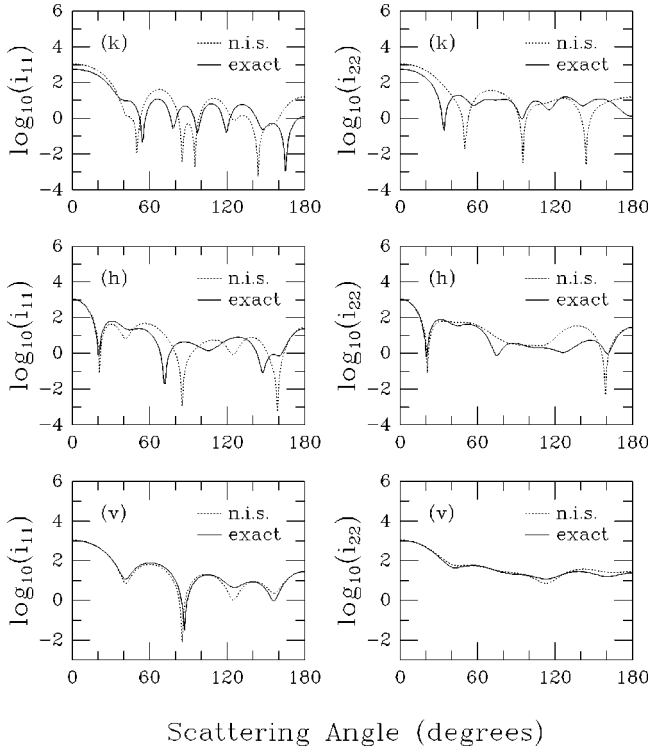

FIG. 21. Same as Fig. 16, but for the target ID No. 542 000 (see Table I).

that the interference effect disappears at $\theta \sim 0°$ or $\theta \sim 180°$. In the case of h, the Mie solutions and the coherent Mie scattering are identical only at $\theta = 0°$ and $\theta = 180°$. Therefore, due to the interference with different phases at different scattering angles, except for $\theta = 0°$ and $\theta = 180°$, the rigorous solution and the coherent Mie scattering have no resemblance unless the interaction between spheres is negligible. Unlike the orientations of v and h where $Z^l \equiv 0$, the scattering at the orientation of k includes the phase term introduced by Z^l. In this case, $\Delta^l = Z^l \cos\theta$. When there is no interac-

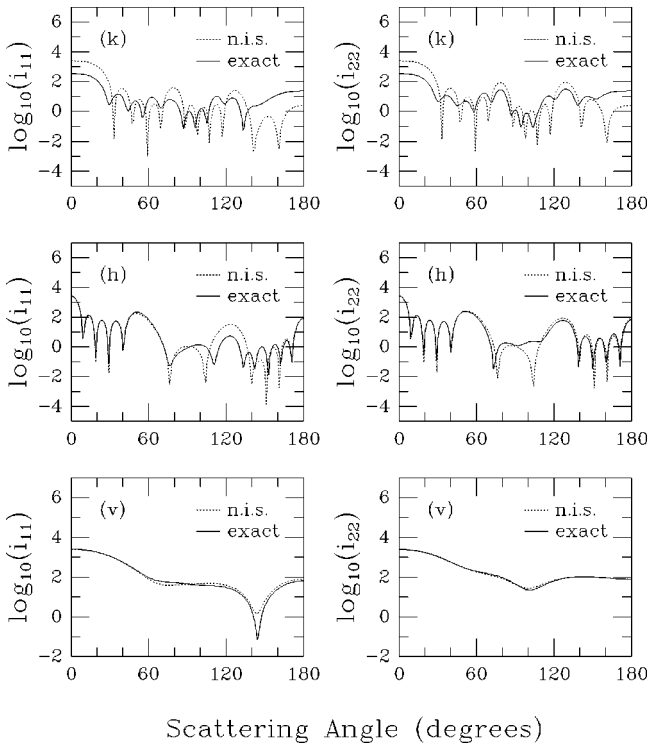

FIG. 20. Same as Fig. 16, but for the target ID No. 535 001 (see Table I).

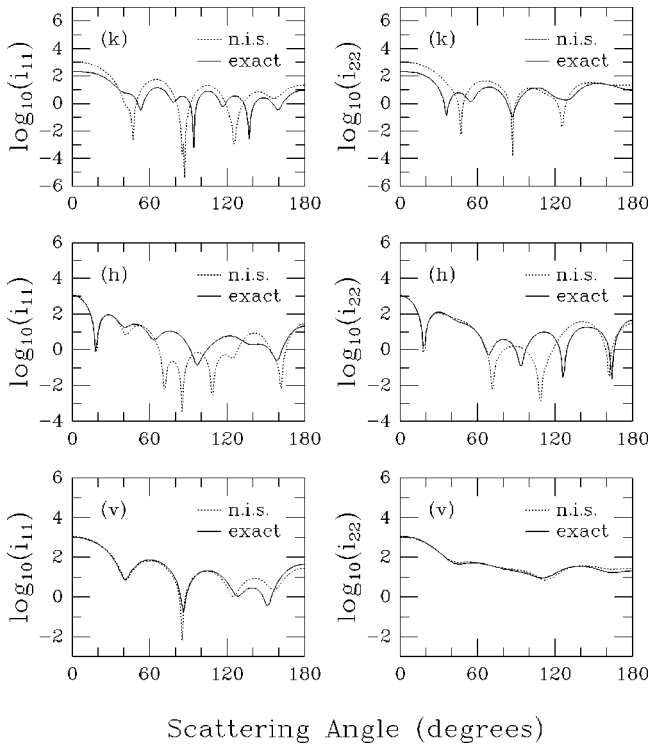

FIG. 22. Same as Fig. 16, but for the target ID No. 542 001 (see Table I).

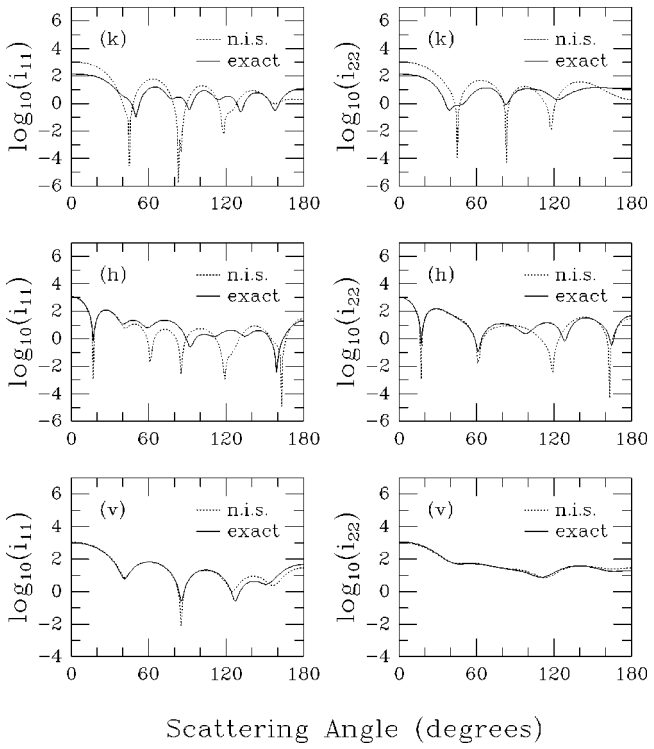

FIG. 23. Same as Fig. 16, but for the target ID No. 542 002 (see Table I).

tion between spheres, the phase factor is virtually $\exp[ikZ^l(1-\cos\theta)]$ for identical spheres, which indicates that the Mie calculations for the single component spheres and the coherent Mie scattering can be identical only at $\theta=0°$. Interaction between spheres destroys the only possible resemblance between rigorous solution and the coherent Mie scattering in the region near this forward scattering direction.

In general, the similarities and the differences between the rigorous and the noninteracting approximate solutions are determined by the phase terms $\exp(-ik\Delta^l)$ and $\exp(-ikZ^l)$ as well as the degree of interaction between spheres. When the axis of symmetry of the chains of spheres deviates from the incident beam direction or is off the scattering plane, the interaction effect becomes much weaker than when it is along the forward direction of $\theta=0°$. This is the reason why on taking average over random orientations the strong interaction between spheres along the beam direction is averaged out by the much weaker interactions at the majority of other orientations.

B. Orientation dependence of scattered intensity at a fixed scattering angle

One of the interesting discoveries in Wang's experimental study of dependent scattering by linear chains of spheres is the dramatic enhancement of the scattered intensity when the chain's axis of symmetry bisects the scattering angle [22]. This so-called specular resonance has been discussed by Kattawar and Dean [31] and by Fuller, Kattawar, and Wang [32]. Figures 24–28 refer to five different aggregates of two identical spheres in contact and show respectively the variation of $i_{11}(\theta=90°)$ with the orientation angle χ, the angle between the dumbbell's axis of symmetry and the incident

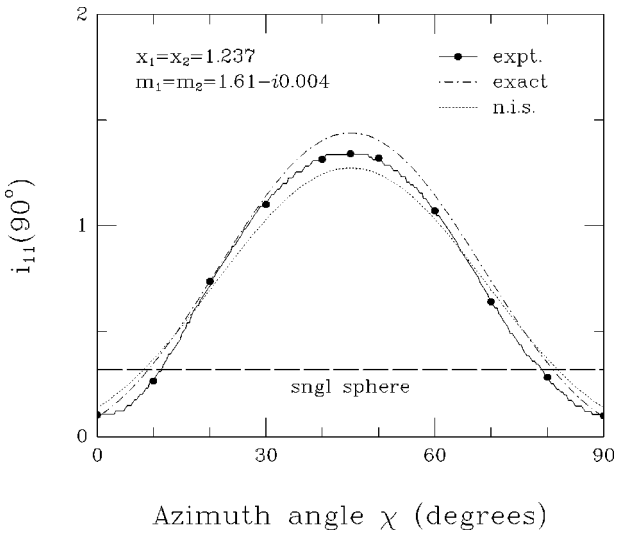

FIG. 24. Comparison of Xu's rigorous solution (exact) and noninteracting coherent Mie scattering NIS with Wang's microwave analog scattering measurements (expt.) for the scattering intensity $i_{11}(90°)$ observed at the fixed scattering angle $\theta=90°$ as a function of the orientation angle χ of two identical spheres in contact. The size parameter (x) and the refractive index of the spheres (m) are shown at the left upper corner. The axis of symmetry of the two spheres is always confined in the scattering plane. When $\chi=0°$, the axis is parallel to the plane incident beam direction, and $\chi=90°$ means that the axis is perpendicular to the incident beam direction. The NIS approximation considers only the interference effect between independent spheres, and the rigorous solution accounts for both the interference and interaction effects. The Mie solution for a single component sphere is also shown, labeled ''sngl sphere.''

beam direction, as the axis is rotated in the scattering plane. Together with the microwave scattering data and the rigorous solution, the coherent Mie-scattering NIS approximation is also shown. The χ dependence of $i_{11}(\theta)$ of two noninteracting identical spheres is very simple, as described by Eq. (24). Again, Figs. 24–28 are examples showing a good agreement between our rigorous solution and scattering measurement. It is noteworthy here that the peak orientation

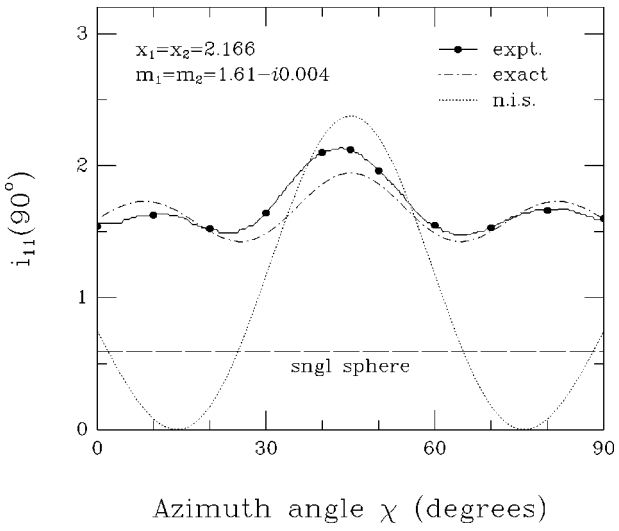

FIG. 25. Same as Fig. 24, but the two identical spheres in contact have a size parameter of 2.166.

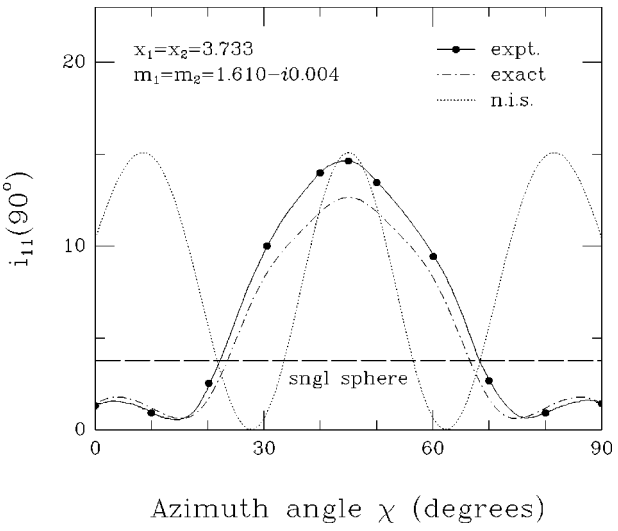

FIG. 26. Same as Fig. 24, but the two identical spheres in contact have a size parameter of 3.733.

angle $\chi=\theta/2$, where the maximum of the scattered intensity occurs, is determined by the interference maximum of the Mie-scattered fields from the two individual spheres. When the size parameter of the individual sphere is small, coherent Mie scattering is close to rigorous solution, as shown in Fig. 24. The larger the size of the individual sphere, the stronger the interaction between the two spheres and the higher the enhancement in the peak scattered intensity. However, the location of χ where the resonance occurs, i.e., $\chi=\theta/2$, seems to be unaffected by the interaction between spheres, as shown by both the theoretical calculation and the experimental results. The reason for this may be that, although the interaction modifies the scattered Mie fields of the two identical component spheres, the difference between the two component scattered fields is not large and the locations of the scattering peaks are still determined by the function represented by Eq. (24).

C. Forward scattering

As mentioned at the end of Sec. II, it is convenient to express the complex scattering amplitude at $\theta=0°$, denoted

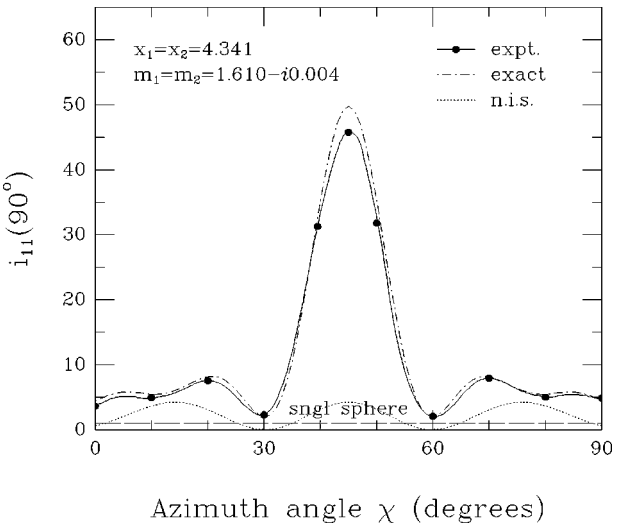

FIG. 27. Same as Fig. 24, but the two identical spheres in contact have a size parameter of 4.341.

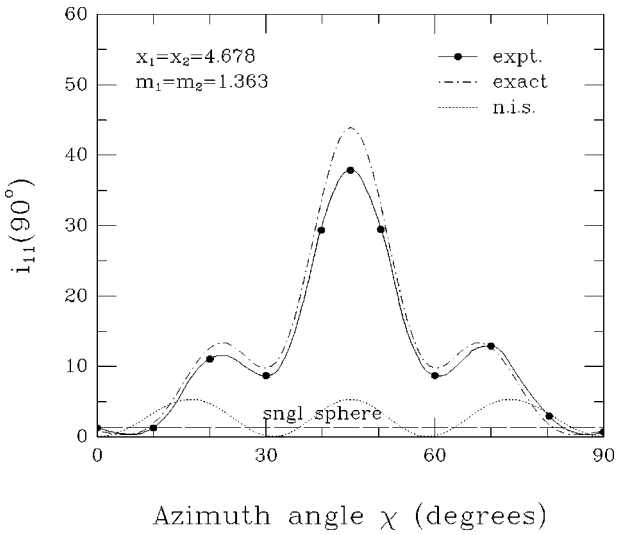

FIG. 28. Same as Fig. 24, but the two identical spheres in contact have a size parameter of 4.678 and the refractive index of 1.363.

by $S(0°)$, in the (P,Q) form, as defined by Eqs. (18). A curve traced out in the (P,Q) plane, as the target's configuration or orientation varies, is called a (P,Q) plot. In this subsection, we compare our $\theta=0°$ theoretical calculations for aggregates of spheres with two groups of microwave measurements, all through (P,Q) plots: (1) the variation of the complex forward scattering amplitude $S(0°)$ as two identical spheres are continuously pulled apart along the incident beam direction, and (2) the target-orientation dependence of $S(0°)$. In these comparisons, we see that the computed and measured (P,Q) graphs are similar only in the general mor-

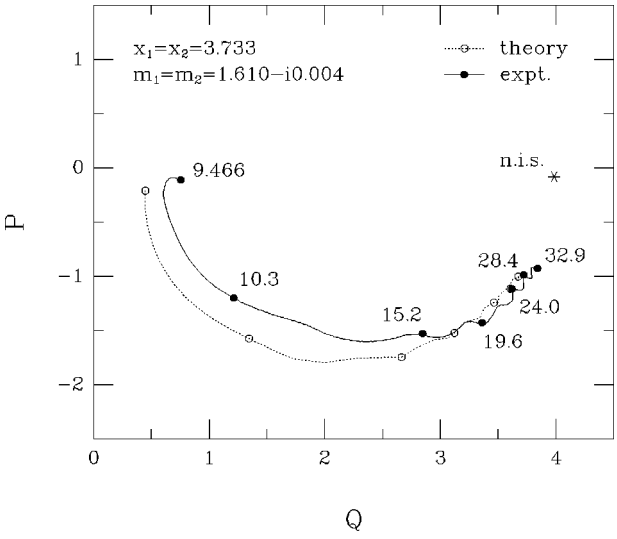

FIG. 29. Theoretical and experimental (P,Q) plots of two identical spheres in continuous separation along the incident beam direction. The size parameter (x) and the refractive index of the spheres (m) are 3.733 and $1.61-i0.004$, respectively. The running numbers denote the dimensionless ''separation parameter'' kd, where d is the separation distance between the two spheres and k is the wave number. The asterisk $*$ marked n.i.s. represents the noninteracting-scattering (NIS) solution, which is the same as the Mie solution for a single component sphere in this case.

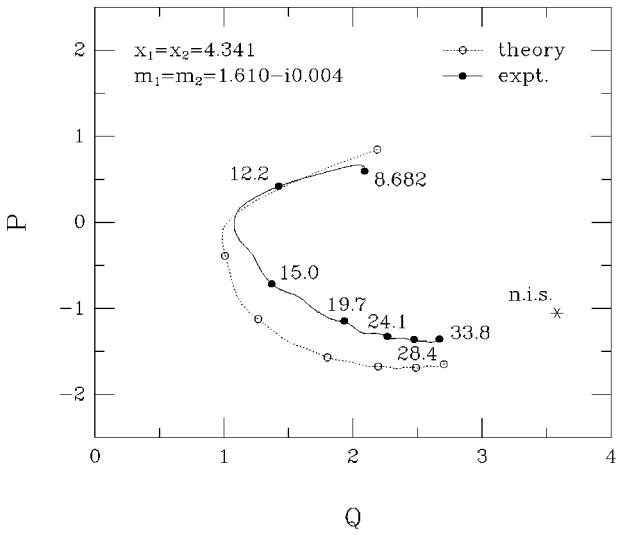

FIG. 30. Same as Fig. 29, but the two identical spheres have a size parameter of 4.341.

phology. As noticed by previous authors [32], the (P,Q) graphs provide the most sensitive test to the experimental data because, as discussed in Sec. IV, an extinction measurement is not only technically difficult to perform but also very sensitive to environmental perturbations during measurement.

1. Continuous separation of two identical spheres along the incident direction

Figures 29–32 refer to four pairs of identical spheres aligned along the z axis, each pair differing from others in the component sphere size or refractive index, and show the variation of $S(0°)$ in the complex (P,Q) plane when the center-to-center separation distance d between the two spheres continuously increases. The size parameter and the refractive index of the component spheres can be found in each figure. The running numbers in these figures denote the dimensionless ''separation parameter'' kd, starting from the minimum value when the two spheres are in contact. As d

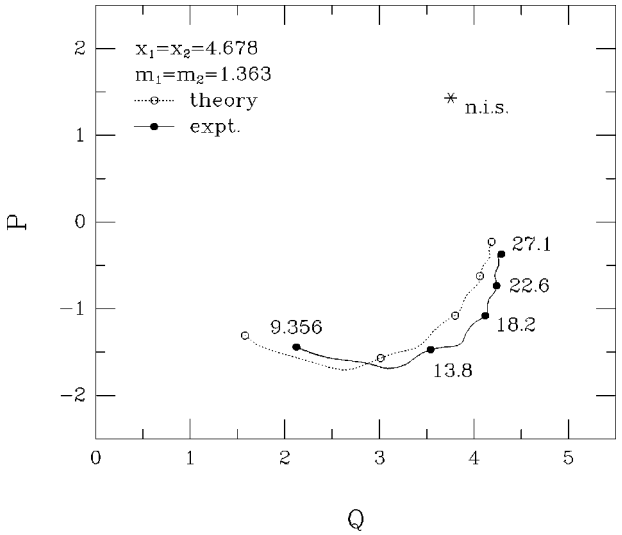

FIG. 31. Same as Fig. 29, but the size parameter of the two identical spheres is 4.678 and their refractive index is 1.363.

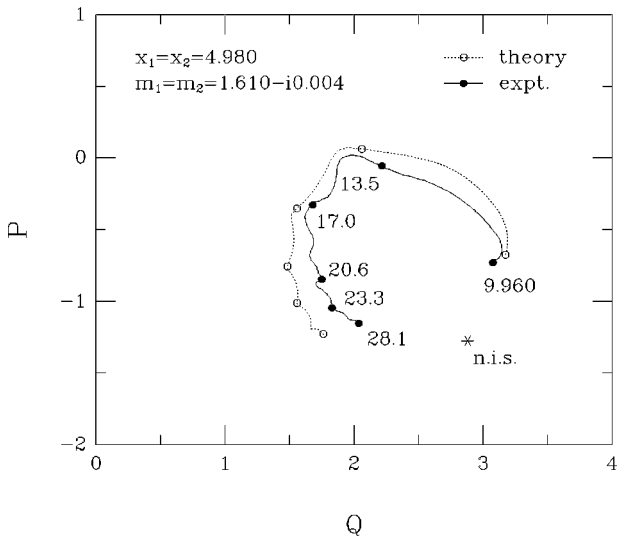

FIG. 32. Same as Fig. 29, but the size parameter of the two identical spheres is 4.980.

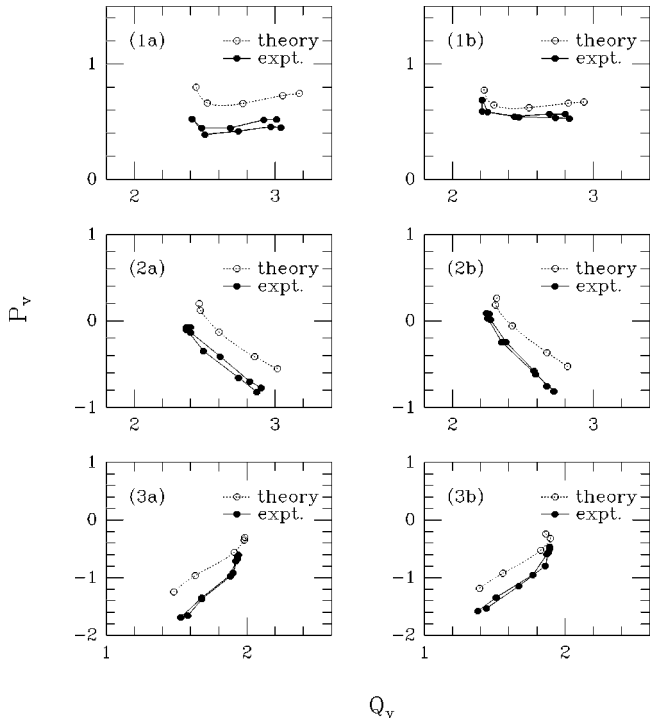

FIG. 33. Theoretical and experimental volume-equivalent (P,Q) plots showing the orientation dependency of the forward scattering at $\theta=0°$ for (a) a contacting square array (left) and (b) a contacting cubic array (right) of four or eight identical spheres of three different sizes. An individual component sphere shown in the top row (1) has the size parameter of 3.12 and the refractive index of 1.365. For the middle (2) and bottom (3) rows, the size parameters are respectively 3.752 and 4.678, and the refractive indexes are, respectively, 1.366 and 1.363. The major difference for the different rows is the size of the spheres. While the top and bottom faces of the sphere arrays are always parallel to the scattering plane, the arrays are continuously rotated in the scattering plane by 90° from the initial orientation angle 0° with two side faces perpendicular to the incident beam direction. The initial and the final (after 90° rotation) orientations are in fact the same for these two particular configurations. The filled and open circles correspond to the measured and computed quantities at the orientation angles from 0° to 90° in a step of 10°.

increases, the tip of $S(0°)$ vector travels in general along a counterclockwise curve, converging toward a limit with an ever-decreasing speed. This limit is equal to $2\hat{S}(0°)$, where $\hat{S}(0°)$ is the forward scattering amplitude of an isolated component sphere, and is represented by an asterisk in the figures. The limit corresponds to the $S(0°)$ vector of two noninteracting spheres, i.e., the NIS solution valid for a sufficiently large kd. We noticed that the theoretical P values have opposite signs to those defined in the experimental data. This is due to the employment of $\exp(-i\omega t)$ as time factor in Xu's theory instead of the $\exp(i\omega t)$ convention [34] followed by the experiment. As a result, the $S(\theta)$ defined in the latter convention is the complex conjugate of that defined in the former. This results in the opposite signs for P but leaves the same (always positive) sign for Q for the two conventions.

2. Orientation-dependence of the forward scattering at $\theta=0°$

The forward scattering amplitude $S(0°)$ depends strongly on the orientation of the target. Figure 33 shows the orientation-dependence of the forward scattering properties for three groups of four- and eight-sphere arrays. The values of (P,Q) shown in the figures, labeled by (P_v,Q_v), are the volume-equivalent quantities defined by $Q=4\pi\ \mathrm{Re}[S(0°)]/(k^2G_v)$ and $P=-4\pi\ \mathrm{Im}[S(0°)]/(k^2G_v)$. G_v is the geometric cross section of a sphere equal in volume to the total of all component spheres in an array. In each of the three groups of different size of identical spheres shown in different rows in Fig. 33, four or eight spheres form arrays of a contacting square or cubic geometry. The top and bottom surfaces of each array are kept parallel to the scattering plane. These arrays are continuously rotated in the scattering plane by 90°, starting from the initial orientation angle 0° where two side surfaces are perpendicular to the incident beam direction. By virtue of the array symmetry, the two parts of the (P,Q) curve in traversing the orientation angle ranges $(0°,45°)$ and $(45°,90°)$, respectively, should be identical. From Fig. 33 we see that the (P,Q) signatures of the eight-sphere cubic array (in the right column) are similar to those of the four-sphere square array (in the left column). This implies that there are no appreciable interference and interaction between the two layers of four spheres in the eight-sphere cubic arrays. This is not surprising in view of the discussion in the Sec. V A *2*.

VI. CONCLUSIONS

As we discuss here, analytical representation of the complex amplitude scattering matrix is essential to an electromagnetic scattering formulation. We have tested our formulation for the amplitude scattering matrix of aggregated particles by the comparison of theoretical results with laboratory scattering measurements. The agreement of theory with experiment is satisfactory for all types of experimental data that we tested: angular distribution of the scattered intensities at random and fixed orientations, the specular resonances of the scattered intensities at a fixed scattering angle, and the forward scattering signatures at the scattering angle of $\theta=0°$. With the interaction between component particles turned off, this scattering formulation describes precisely the coherent scattering by independent particles. When the number of particles and the sizes of the component particles in an ensemble are both small, the noninteracting scattering is a good approximation to the rigorous solution, especially for an average over random orientations. The strongest interaction occurs when the component particles are aligned along the direction of propagation of the incident radiation.

In summary, we have confirmed here by the experimental scrutiny the analytical representation of the amplitude scattering matrix developed recently from the far-field solution of the multisphere-scattering problem and thus the multisphere scattering formulation derived therefrom.

ACKNOWLEDGMENTS

This study was supported in part by the National Science Foundation through Grant No. AST-9619539. One of the authors (R.W.) sincerely thanks Professor J. M. Greenberg, founder of the microwave analog scattering facility in the late 1950s, for his long-term support and encouragement.

[1] B. Friedman and J. Russek, Q. Appl. Math. **12**, 13 (1954).
[2] S. Stein, Q. Appl. Math. **19**, 15 (1961).
[3] O. R. Cruzan, Q. Appl. Math. **20**, 33 (1962).
[4] C. Liang and Y. T. Lo, Radio Sci. **2**, 1481 (1967).
[5] J. H. Bruning and Y. T. Lo, IEEE Trans. Antennas Propag. **19**, 378 (1971).
[6] J. H. Bruning and Y. T. Lo, IEEE Trans. Antennas Propag. **19**, 391 (1971).
[7] A. Goyette and A. Navon, Phys. Rev. B **13**, 4320 (1976).
[8] F. Borghese, P. Denti, G. Toscano, and O. I. Sindoni, Appl. Opt. **18**, 116 (1979).
[9] J. M. Gérardy and M. Ausloos, Phys. Rev. B **25**, 4204 (1982).
[10] F. Borghese, P. Denti, R. Saija, G. Toscano, and O. I. Sindoni, Aerosol. Sci. Technol. **4**, 227 (1984).
[11] K. A. Fuller and G. W. Kattawar, Opt. Lett. **13**, 90 (1988).
[12] K. A. Fuller and G. W. Kattawar, Opt. Lett. **13**, 1063 (1988).
[13] A-K. Hamid, I. R. Ciric, and M. Hamid, Can. J. Phys. **68**, 1419 (1990).
[14] D. W. Mackowski, Proc. R. Soc. London, Ser. A **433**, 599 (1991).
[15] D. W. Mackowski, J. Opt. Soc. Am. A **11**, 2851 (1994).
[16] K. A. Fuller, J. Opt. Soc. Am. A **11**, 3251 (1994).
[17] Y.-l. Xu, Appl. Opt. **34**, 4573 (1995).
[18] Y.-l. Xu, Appl. Opt. **36**, 9496 (1997).
[19] Y.-l. Xu, Phys. Lett. A (to be published).
[20] C. F. Bohren and D. R. Huffman, *Absorption and Scattering of Light by Small Particles* (Wiley, New York, 1983).
[21] R. T. Wang, in *Light Scattering by Irregularly Shaped Particles*, edited by D. W. Schuerman (Plenum, New York, 1980), pp. 255–272.
[22] R. T. Wang, J. M. Greenberg, and D. W. Schuerman, Opt. Lett. **6**, 543 (1981).

[23] D. W. Schuerman and R. T. Wang, U.S. Army CSL Contractor Report No. ARCSL-CR-81003, 1981.
[24] R. T. Wang and D. W. Schuerman, in *Proceedings of the 1981 CSL Scientific Conference on Obscuration and Aerosol Research,* edited by R. Kohl (U.S. Army Chemical Systems Laboratory, Aberdeen Proving Ground, Maryland, 1982), pp. 47–58.
[25] R. T. Wang, in *Proceedings of the 1982 CSL Scientific Conference on Obscuration and Aerosol Research,* edited by R. Kohl (U.S. Army Chemical Systems Laboratory, Aberdeen Proving Ground, Maryland, 1983), pp. 223–242.
[26] R. T. Wang, in *Proceedings of the 1983 CRDC Scientific Conference on Obscuration and Aerosol Research,* edited by J. Farmer and R. Kohl (U.S. Army Chemical Research and Development Center, Aberdeen Proving Ground, Maryland, 1984), pp. 223–235.
[27] R. T. Wang and B. Å. S. Gustafson, in *Proceedings of the 1983 CRDC Scientific Conference on Obscuration and Aerosol Research,* edited by J. Farmer and R. Kohl (U.S. Army Chemical Research and Development Center, Aberdeen Proving Ground, Maryland, 1984), pp. 237–247.
[28] R. T. Wang, in *Proceedings of the 1984 CRDC Scientific Conference on Obscuration and Aerosol Research,* edited by J. Farmer and D. Stroud (U.S. Army Chemical Research and Development Center, Aberdeen Proving Ground, Maryland, 1985), pp. 315–326 and 327–363.
[29] R. T. Wang, in *Proceedings of the 1987 CRDEC Scientific Conference on Obscuration and Aerosol Research,* edited by E. H. Engquist and K. A. Sistek (U.S. Army Chemical Research, Development and Engineering Center, Aberdeen Proving Ground, Maryland, 1988), pp. 323–339.
[30] R. T. Wang and H. C. van de Hulst, Appl. Opt. **34**, 2811 (1995).
[31] G. W. Kattawar and C. E. Dean, Opt. Lett. **8**, 48 (1983).
[32] K. A. Fuller, G. W. Kattawar, and R. T. Wang, Appl. Opt. **25**, 2521 (1986).
[33] W. J. Wiscombe, Appl. Opt. **19**, 1505 (1980).
[34] H. C. van de Hulst, *Light Scattering by Small Particles* (Wiley, New York, 1957).
[35] M. Kerker, *The Scattering of Light and Other Electromagnetic Radiation* (Academic, New York, 1969).
[36] Y.-l. Xu, Math. Comput. **65**, 1601 (1996).
[37] Y.-l. Xu, J. Comput. Phys. **127**, 285 (1996); Erratum, *ibid.* **134**, 200 (1997).
[38] Y.-l. Xu, J. Comput. Appl. Math. **85**, 53 (1997).
[39] Y.-l. Xu and B. Å. S. Gustafson, Appl. Opt. **36**, 8026 (1997).
[40] Y.-l. Xu, J. Comput. Phys. **139**, 137 (1998).
[41] J. M. Greenberg, in *Light Scattering by Irregularly Shaped Particles,* edited by D. W. Schuerman (Plenum, New York, 1980), pp. 7–24.
[42] J. A. Stratton, *Electromagnetic Theory* (McGraw-Hill, New York, 1941).
[43] S. Roberts and A. von Hippel, J. Appl. Phys. **17**, 610 (1946).